


RESEARCH

Open Access



# A probabilistic geologic model of the Krafla geothermal system constrained by gravimetric data

Samuel W. Scott<sup>1\*</sup> , Cari Covell<sup>1</sup>, Egill Júlíusson<sup>2</sup>, Águst Valfell<sup>1</sup>, Juliet Newson<sup>1</sup>, Birgir Hrafnkelsson<sup>3</sup>, Halldór Pálsson<sup>3</sup> and María Gudjónsdóttir<sup>1</sup>

\*Correspondence:

samuels@ru.is

<sup>1</sup> Department of Engineering, Reykjavik University, Menntavegur 1, 101 Reykjavik, Iceland  
Full list of author information is available at the end of the article

## Abstract

The quantitative connections between subsurface geologic structure and measured geophysical data allow 3D geologic models to be tested against measurements and geophysical anomalies to be interpreted in terms of geologic structure. Using a Bayesian framework, geophysical inversions are constrained by prior information in the form of a reference geologic model and probability density functions (pdfs) describing petrophysical properties of the different lithologic units. However, it is challenging to select the probabilistic weights and the structure of the prior model in such a way that the inversion process retains relevant geologic insights from the prior while also exploring the full range of plausible subsurface models. In this study, we investigate how the uncertainty of the prior (expressed using probabilistic constraints on commonality and shape) controls the inferred lithologic and mass density structure obtained by probabilistic inversion of gravimetric data measured at the Krafla geothermal system. We combine a reference prior geologic model with statistics for rock properties (grain density and porosity) in a Bayesian inference framework implemented in the GeoModeller software package. Posterior probability distributions for the inferred lithologic structure, mass density distribution, and uncertainty quantification metrics depend on the assumed geologic constraints and measurement error. As the uncertainty of the reference prior geologic model increases, the posterior lithologic structure deviates from the reference prior model in areas where it may be most likely to be inconsistent with the observed gravity data and may need to be revised. In Krafla, the strength of the gravity field reflects variations in the thickness of hyaloclastite and the depth to high-density basement intrusions. Moreover, the posterior results suggest that a WNW–ESE-oriented gravity low that transects the caldera may be associated with a zone of low hyaloclastite density. This study underscores the importance of reliable prior constraints on lithologic structure and rock properties during Bayesian geophysical inversion.

**Keywords:** Geologic modeling, Bayesian inference, Gravity, Iceland

## Introduction

Three-dimensional (3D) geologic models illustrate the spatial distribution of subsurface lithologic units and major structural features such as faults, and visually convey geoscientific understanding during the process of resource assessment and conceptual model development. The models are based on a combination of geologic data derived from surface geologic mapping and boreholes as well as indirect evidence from geophysical, hydrologic or other measurements. Geophysical data sets (e.g., gravity potential field) may be calculated directly from 3D geologic models by assigning values for petrophysical properties (e.g., density) to the subsurface rock units and calculating the forward gravity model. The quantitative links between geology and geophysics may allow a geologic model to be tested against measured geophysical data sets, as well as the interpretation of geophysical anomalies in terms of geologic structure. However, all 3D geologic models are based on input parameters prone to potentially large uncertainties. Geophysical inversion results describing the distribution of rock types and physical property values in the subsurface are also uncertain, as an infinite number of possible models of the subsurface may account for the measured data. While the integration of geologic constraints and prior information such as rock petrophysical properties are necessary to ensure the inversion process retains geologic meaning, overly strong constraints may lead to an underestimation of uncertainty in the final results. Quantifying how the degree of confidence in the prior understanding of geothermal system structure affects results from probabilistic inversion methods is necessary for these approaches to contribute to effective risk management in geothermal resource assessment (United Nations Economic Commission for Europe Expert Group on Resource Classification 2017).

Geophysical measurements can be used to test existing geologic models and infer the properties of the subsurface in areas where primary observational data from boreholes are lacking. Given a prior model of the subsurface, inversion improves the correspondence between measured data and the calculated geophysical data (reduces the misfit) by adjusting the structure and properties of that model. Deterministic inversion methods calculate a solution that minimizes this misfit by modifying only the physical properties of the model cells specified in the initial model (Li and Oldenburg 1998) and/or by modifying the rock type (and indirectly, the physical properties) of the model cells (Fulgagar et al. 2008). As inversion of gravity potential field data is highly under-constrained (a phenomenon termed non-uniqueness in geophysical inverse theory), the a priori constraints on the geometric arrangement of the main rock units and their petrophysical properties in the initial model play a critical role in retaining geological meaning in the inversion process (Boulianger and Chouteau 2001; Li and Oldenburg 1998). To account for the uncertainty of the geometry of the initial model itself and the physical properties of each rock type, manual adjustment of the initial model geometry and/or rock properties is typically performed to assess their effect on the inversion results (e.g., Abdelfettah et al. 2014; Altwegg et al. 2015; Miller et al. 2017; Witter et al. 2016).

Probabilistic inversion methods are becoming increasingly popular as geologic modeling becomes integrated into advanced machine-learning and Bayesian inference frameworks (Calcagno et al. 2008; De La Varga et al. 2019; Jessell et al. 2014). These techniques generate millions of possible realizations of subsurface structure from a reference prior model by stochastically varying lithologic structure and rock

physical properties according to specified prior probability distributions. Similar to deterministic techniques, a geologic model configuration is considered more likely if it is consistent with prior geologic information about the system and it reduces the misfit between the forward-modeled geophysical field and measured data. However, in contrast to deterministic inversion techniques, such approaches provide posterior probability distributions for rock type and corresponding rock properties over the model space (Bosch 1999; Bosch et al. 2001; Chen et al. 2012; Corbel and Wellmann 2015; De La Varga et al. 2015; Guillen et al. 2008; Jessell et al. 2014; McCalman et al. 2014; Wellmann et al. 2017). Although the mode of the posterior might be seen as the most probable model, analogous to a global optimum solved using deterministic inversion, probabilistic models should not be used to infer a single structure but rather to falsify a range of possible models inconsistent with observations (Tarantola 2006).

The non-uniqueness of gravity potential field data means that an infinite number of possible realizations of the subsurface density structure may be consistent with measured data. This partially makes Bayesian inference methods well-suited for the inversion of gravity potential field data, since they allow a prior model of the distribution of rock types and density to reflect the additional knowledge gained about the subsurface through the gravity data. The prior beliefs are updated based on a likelihood probability, which describes a probabilistic relationship between model and data and is based on knowledge of physical laws and measurement error. Although the uncertainty of the gravity data may be significant, the more difficult uncertainty to account for in Bayesian inversion of geophysical data is the uncertainty of the prior (e.g., Caers 2011; Scales and Tenorio 2001). While an overly conservative prior will restrict the possible solution space and lead to underestimation of uncertainty, an overly broad prior will produce geologically meaningless results.

In this study, we develop a probabilistic geologic model of the Krafla geothermal field constrained by gravimetric data. Our approach combines 3D geologic modeling, statistical analyses of rock properties, and inversion of gravimetric data to assess the lithologic and density structure of a volcanic geothermal system. The Bayesian inference framework, implemented in GeoModeller V4 (Intrepid Geophysics 2017a), uses Markov Chain Monte Carlo sampling to calculate the posterior probability densities for the model parameters lithology and bulk density in light of the observed gravity data. We incorporate two forms of empirical prior information about the Krafla system, a reference geological model developed by expert geologists (Mortensen et al. 2009; Weisenberger et al. 2015), and probability distributions describing the bulk mass densities of the main rock types based on statistical analyses of laboratory measurements. Our main objective is to assess how treatment of uncertainty in the reference prior geologic model and petrophysical properties affects the probabilistic inversion results. In addition to varying the structure of the reference prior model and the prior physical properties of the main rock types, we explore how posterior results are affected by the probability that lithologic changes are proposed to the reference model and the strength of the applied geologic constraints. We show how the uncertainty of the prior exerts a strong control on posterior results, and suggest that treating this uncertainty as a variable that is varied

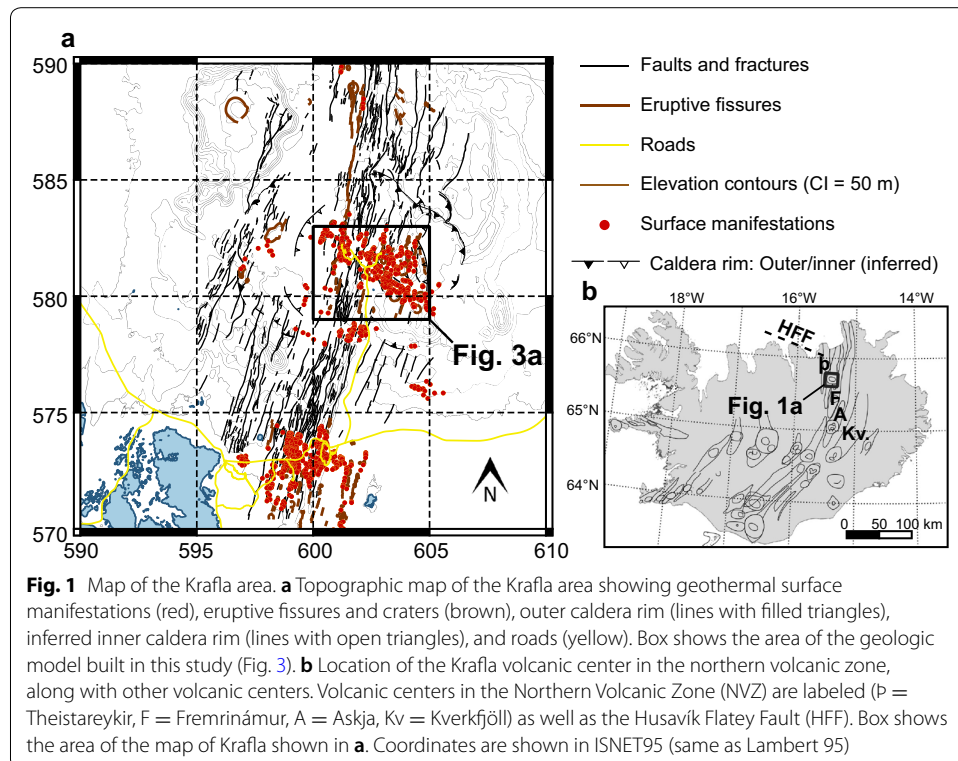
between inversion runs may allow the most uncertain parts of the reference prior model to be determined.

### Krafla geothermal field

Krafla is one of five active volcanic centers arranged in en-echelon fashion within the northern volcanic zone (NVZ) in northeast Iceland, along with Kverkfjöll, Askja, Fremrinámur and Theistareykir (Fig. 1). To the north, the NVZ joins with the Husavik Flatey Fracture Zone (HFFZ), a right-lateral transform zone that connects the NVZ with the Kolbeinsey Ridge north of Iceland. To the south, a left-lateral transform zone, the South Iceland Seismic Zone (SISZ), conveys the divergent plate boundary and locus of crustal extension and volcanism towards the west. The Krafla area features a volcanic caldera astride a major NNE–SSW trending fissure swarm (Sæmundsson 2008). While volcanism in the caldera dominantly occurs as basaltic fissure eruptions and dike injections, there are intermittent eruptions of more silicic magmas (Jónasson 1994). A large earthquake sequence accompanied by repeated dike injections and basaltic fissure eruptions occurred in 1975–1984, mostly in the northern part of the fissure swarm (Björnsson et al. 1977; Einarsson 1991). In the center part of the caldera, where geothermal surface manifestations are abundant (Fig. 1b), the area hosts a geothermal power plant that currently generates 60 MWe.

### Geologic structure

The geologic structure of the Krafla area has been intensively studied (Ármannsson et al. 1987; Mortensen et al. 2009; Pope et al. 2016; Sæmundsson 1991, 2008; Stefánsson 1981;

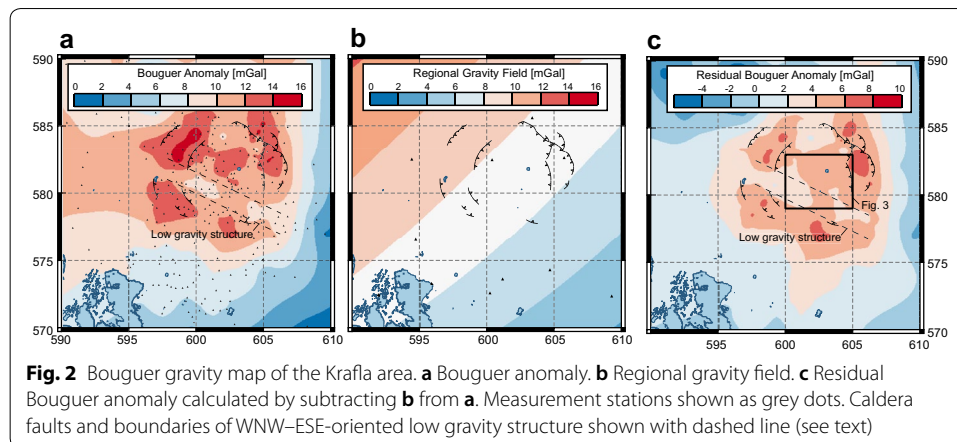


Weisenberger et al. 2015). The subsurface geology mainly consists of alternating layers of sub- or intraglacially-erupted basaltic hyaloclastite (a broad term describing highly heterogeneous rocks consisting of a mix of breccias, tuffs and pillow basalts) and subaerially-erupted basaltic lava flows in the upper 1.5 km with interspersed basaltic dikes and sills and rhyolitic intrusions. Doleritic and gabbroic intrusions become increasingly pervasive below 1.5 km depth, along with minor granophyre and other silicic intrusions. The alteration mineralogy follows a typical temperature-dependent zonation with depth (Kristmannsdóttir 1979; Sveinbjörnsdóttir 1992). With increasing depth and temperature, these zones are the smectite–zeolite zone, the mixed-layer clay zone, the chlorite–epidote zone, the epidote zone, and the epidote–actinolite zone. Multiple lines of evidence suggest the presence of a network of basaltic sills and dykes at depths of ~ 3–7 km beneath the Krafla caldera (e.g., Brandsdóttir et al. 1997; de Zeeuw-van Dalfsen et al. 2006; Einarsson 1978; Kennedy et al. 2018; Tryggvason 1986), and direct evidence of rhyolitic magma was provided during the drilling of the IDDP-1 well, which encountered a rhyolitic intrusion formed by partial melting of hydrothermally altered basalts at ~ 2.1 km depth (Elders et al. 2011, 2014).

### Gravity potential field

Gravimetric data measures spatial variations in Earth's gravitational field (usually restricted to the vertical component of the gravitational field) resulting from density contrasts in the subsurface. Several gravity surveys have been carried out at Krafla between 1969 and 2015 (Johnsen et al. 1980; Johnsen 1995; Magnússon 2016). The gravity data used in this study is described in detail by Magnússon (2016), which considers 522 measurements made over an area of ~ 625 km<sup>2</sup>. Station spacing is highly variable, ranging from 0.1 to ~ 10 km, with a total of 49 stations located within the 20 km<sup>2</sup> area of the geologic model. The Bouguer anomaly is calculated assuming a reference density of 2.51 g cm<sup>-3</sup>, following Magnússon (2016), and is shown in Fig. 2a. The selected reduction density is also consistent with Kaban et al. (2002). To isolate gravity anomalies resulting from local density heterogeneities within the model domain (restricted to <3 km b.s.l. depth), the residual Bouguer anomaly is calculated by subtracting a regional field (Fig. 2b) estimated by fitting a third-degree polynomial trend to longer-wavelength signals from the Bouguer anomaly. The calculated residual Bouguer anomaly was interpolated onto a regular grid with a resolution of 0.1 km × 0.1 km (Fig. 2c).

The residual Bouguer anomaly reveals a high gravity anomaly associated with the Krafla volcano. High gravity anomalies near the outer caldera rims (6–8 mGal) transition to lower values in the center of the central volcano (3–5 mGal). The gravity data also show a WNW–ESE trending gravity low (shown with white dashed lines in Fig. 2c) that transects the center of the caldera. Árnason et al. (2007) suggest that these trends result from variations in hyaloclastite thickness, inferring the existence of an inner caldera with thicker hyaloclastite piles buried within the outer caldera. Additionally, Árnason et al. (2007) postulate that the WNW–ESE trending gravity low represents an oblique transform graben containing a greater thickness of hyaloclastite. Weisenberger et al. (2015) suggest that this structure plays a major role in the conceptual model of the field, as the deep intrusive heat sources are aligned with this structure and inclined towards the north.



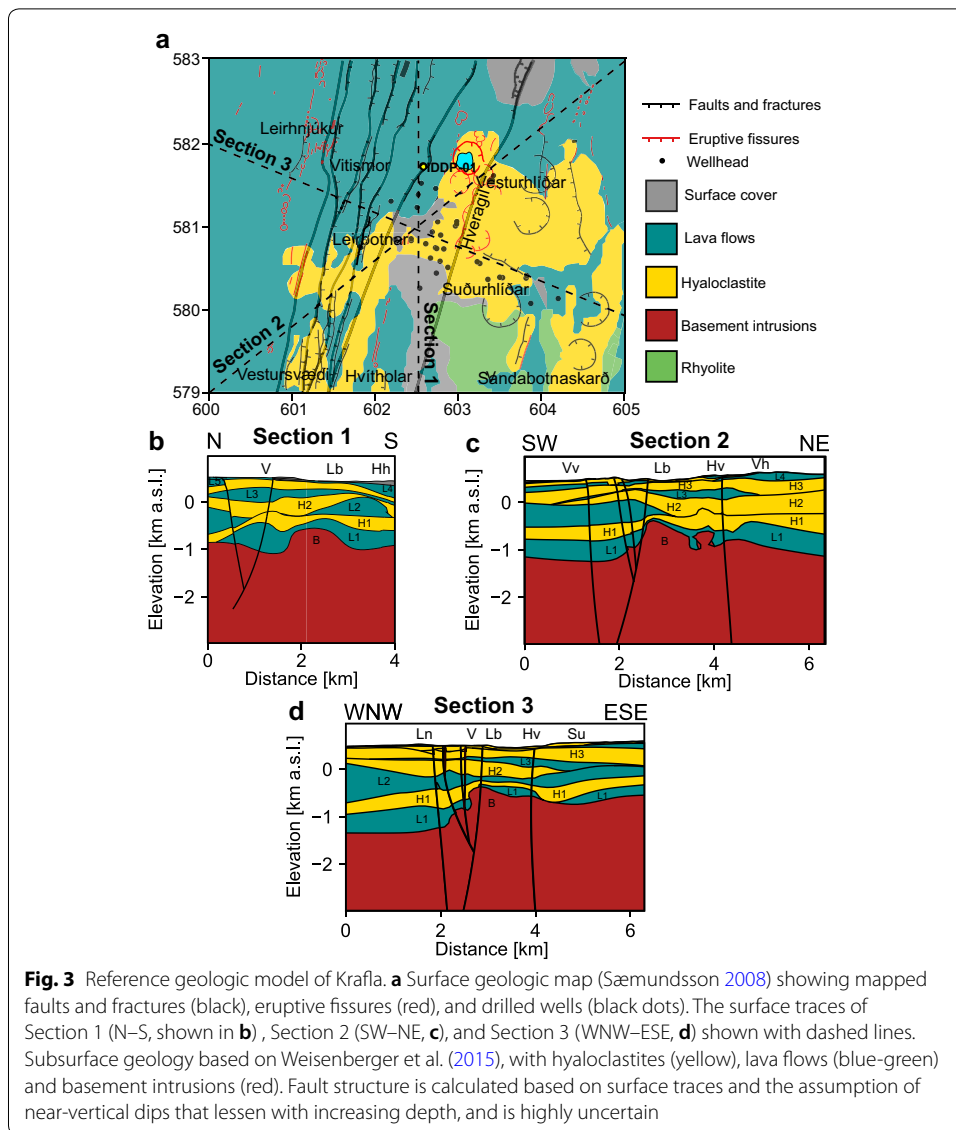
## Methodology

Our approach combines a reference prior geologic model of Krafla built from borehole data and statistics for rock petrophysical properties within a Bayesian inference scheme implemented in the geologic modeling package GeoModeller (Intrepid Geophysics 2017a, b).

### Reference prior geologic model

A reference prior geologic model of the Krafla system was developed based on surface geologic mapping (Sæmundsson 2008) and an interpreted 3D geologic model for the system previously built in Petrel and described by Mortensen et al. (2009) and Weisenberger et al. (2015). The stratigraphic data underlying the reference prior model is derived from 14 wellbores (KS-1, KV-1, K-4, K-8, K-10, K-18, K-19, K-21, K-22, K-24 to K-27, K-30 to K-40 and IDDP-1). GeoModeller uses an implicit approach to calculate the structure of the reference prior model based on contact point and orientation measurements, with lithologic interfaces calculated as a series of multiple interacting scalar potential fields estimated using a co-Kriging geostatistical interpolation scheme (Calcagno et al. 2008).

Figure 3 shows the surface geology within the model domain (the area of which is shown by the white box in Fig. 1a) as well as the location of cross sections, as shown in Fig. 3b–d. The reference geologic model presents a simplified interpretation of the complex sequence of lithologic units identified from well cuttings (Mortensen et al. 2009, and references therein). The 11 stratigraphic units consist of an alternating sequence of five lava flow units (L1–L5, shown in blue) and four hyaloclastite units (H1–H4, yellow) underlain by basement intrusions (B, red) and overlain in some areas by a thin ( $\leq 0.2$  km) surface cover (grey). Although the total area of the geologic model is 25 km<sup>2</sup>, most of the wellbore data, upon which the geologic model is based, is derived from a smaller area in the center of the model (wellbore locations shown by the black dots in Fig. 2a). The two main wellfields, Leirbotnar in the northwest and Suðurhlíðar in the southeast, are separated by a series of explosive craters called Hveragil (Fig. 2a).



Fault structure within the rift zone was calculated based on mapping of selected surface traces (Sæmundsson 2008). Fractures and eruptive fissures strike N to NNE, and show near-vertical dip at the surface that lessens with depth with total throw less than 20 m (Gudmundsson 1989; Hjartardóttir et al. 2012; Opheim and Gudmundsson 1989). Although the calculated fault network is highly uncertain and represents only one possible interpretation, faults are not explicitly included in the litho-constrained inversion scheme implemented in GeoModeller (Intrepid Geophysics 2017b), as the reference prior model is discretized into voxels in which density and lithology are uniform. However, the presence of faults in the model is reflected indirectly in the lithologic structure of the model by lateral changes in the depth of rock layers, which could be possibly indicative of fault displacement, and are included in the presentation of the results for visual convenience. For an explicit consideration

of fault uncertainties in a Bayesian inversion of geophysical data, a useful approach is that of Wellmann et al. (2017).

### Rock properties

Statistics for grain density and total porosity of the main lithologic units were derived from previous studies of Icelandic rock properties and compiled into the Valgarður database (Franzson 2001; Franzson et al. 2010; Frolova et al. 2005, Sigurðsson et al. 2000). The samples were collected mainly between 1992 and 2004 from eroded fossil geothermal systems exposed near the surface and to a lesser extent from cores taken from active geothermal systems. Thus, it is assumed that the petrophysical properties of rock samples are not significantly changed by the process of erosion and exhumation. The data was treated with the purpose of obtaining grain density and total porosity values that also meet the criteria of corresponding to a unique sample ID with a description of the rock type. Based on the rock descriptions, the samples were grouped into the three lithologic types considered in the geologic model:

- hyaloclastite, encompassing sub-glacially erupted breccias, tuffs, and pillow basalts,
- sub-aerially erupted basaltic lavas,
- basement intrusions, including doleritic dykes and sills crystallized at depth as well as gabbroic intrusions.

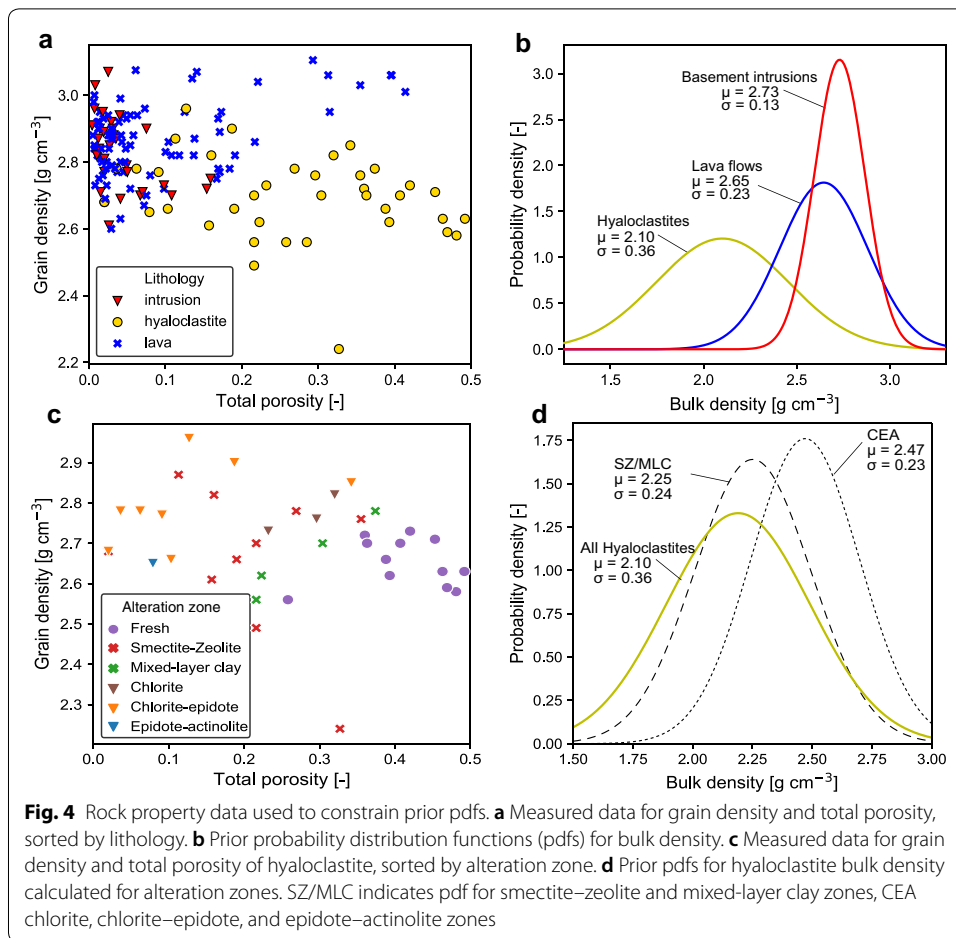
The measured data for grain density and total porosity are shown in Fig. 4a. Hyaloclastites have a slightly lower average grain density ( $2.69 \pm 0.13 \text{ g cm}^{-3}$ ) than the lava flows ( $2.87 \pm 0.11 \text{ cm}^{-3}$ ) and basement intrusions ( $2.75 \pm 0.18 \text{ cm}^{-3}$ ). However, the porosity of hyaloclastites is much higher ( $0.25 \pm 0.14$  compared to  $0.08 \pm 0.1$  for lava flows and  $0.03 \pm 0.04$ , respectively). The statistics for grain density and porosity were used to calculate bulk wet density based on the mass-weighted contributions of the solid rock matrix and fluid in the pore space:

$$\rho_{\text{bulk}} = (1 - \phi)\rho_r + \phi\rho_f, \quad (1)$$

where  $\phi$  is porosity,  $\rho_r$  is grain density, and  $\rho_f$  is fluid density. The bulk wet density (hereafter referred to as bulk density) of each lithology was calculated by fitting a normal and beta probability density function (pdf) to be measured grain density and total porosity, respectively, and performing Monte Carlo sampling of these pdfs to evaluate Eq. 1. The beta distribution for porosity was restricted to values less than 0.6, greater than the maximum porosity value observed in the data. A constant fluid density of  $0.8 \text{ g cm}^{-3}$  (corresponding to  $\sim 250 \text{ }^\circ\text{C}$  pure water) was assumed in the calculation of bulk density. This assumption is a limitation of our model that contributes to greater uncertainty of the prior, as fluid density in geothermal systems can vary strongly, mainly related to variations in the vapor content of boiling zones.

The prior pdfs for the bulk density of each rock type are calculated by fitting a normal distribution to 10,000 samples obtained through the Monte Carlo sampling of Eq. 1, and are shown in Fig. 4b. The bulk density of hyaloclastite ( $2.1 \pm 0.36 \text{ g cm}^{-3}$ ) is much lower than lava flows ( $2.65 \pm 0.23 \text{ g cm}^{-3}$ ) or basement intrusions ( $2.73 \pm 0.13 \text{ g cm}^{-3}$ ), reflecting the high porosity of hyaloclastites. The thin surface





cover has a maximum thickness  $< 0.2$  km and was assigned a bulk density equal to the reference density used in calculation of the Bouguer anomaly ( $2.51 \pm 0.10 \text{ g cm}^{-3}$ ).

The precipitation of secondary minerals in vesicles as well as the replacement of primary basaltic minerals by secondary minerals, mainly clay minerals, may lead to a reduction of porosity and increase in grain density of hyaloclastite (Frolova et al. 2005; Franzson et al. 2010). To account for the effects of alteration, the prior pdfs for the bulk density of the hyaloclastite units were adjusted in some inversion runs to reflect the possible effects of alteration. Figure 4c shows the data for grain density and total porosity of hyaloclastites grouped into the five temperature-dependent alteration zones typically found in Iceland (Kristmannsdóttir 1979; Sveinbjörnsdóttir 1992), as well as the data for fresh (unaltered) hyaloclastites. Altered hyaloclastites containing significant amounts of chlorite, epidote, and actinolite have undergone fluid–rock interaction at temperatures greater than  $240\text{--}250$  °C (Kristmannsdóttir 1979) and show higher grain density ( $2.78 \pm 0.9 \text{ g cm}^{-3}$ ) and lower porosity ( $0.16 \pm 0.11$ ) than hyaloclastites altered to smectite–zeolite or mixed-layer clay facies ( $2.66 \pm 0.16 \text{ g cm}^{-3}$ ,  $0.22 \pm 0.1$ ). The only measurements of total porosity  $> 0.4$  are in fresh hyaloclastites, which are unlikely to be found in the subsurface ( $>0.5$  km depth) in active geothermal areas. Figure 4d shows two normal pdfs for

the bulk density calculated for altered hyaloclastites, with one pdf representing the smectite–zeolite and mixed-layer clay (SZ-MLC) alteration zones ( $2.25 \pm 0.24$ ) and another the chlorite, chlorite–epidote and epidote–actionlite (CEA) alteration zones ( $2.47 \pm 0.23$ ). For the inversion runs accounting for the effects of alteration on hyaloclastite bulk density, we specify a bimodal Gaussian prior pdf in which the proportion of the CEA component increases from 25% near the surface (hyaloclastite unit H4) to 100% in the deepest hyaloclastite unit (H1).

### Bayesian inference framework

GeoModeller uses a Markov Chain Monte Carlo (MCMC) statistical sampling scheme to drive the litho-constrained 3D inversion process and evaluate the posterior probability distribution. The method has been described previously in detail (Bosch 1999; Bosch et al. 2001; Guillen et al. 2008) and will therefore only be briefly summarized here. The Bayesian inference scheme divides the prior probability space into two model parameter spaces:

- a primary geologic parameter space  $\mathbf{m}_{\text{pri}}$  describing the spatial distribution of the lithologies,
- a secondary parameter space  $\mathbf{m}_{\text{sec}}$  describing rock petrophysical properties conditional on lithology.

Measurements of the gravity potential field constitute the additional information about the system used to estimate the posterior probability density functions for lithology and density throughout the model domain according to a modified version of Bayes' law:

$$\pi(\mathbf{m}_{\text{sec}}, \mathbf{m}_{\text{pri}} | y) = cL(y | \mathbf{m}_{\text{sec}})\pi_{s|p}(\mathbf{m}_{\text{sec}} | \mathbf{m}_{\text{pri}})\pi_p(\mathbf{m}_{\text{pri}}), \quad (2)$$

where the posterior pdf,  $\pi(\mathbf{m}_{\text{sec}}, \mathbf{m}_{\text{pri}} | y)$  represents the updated knowledge about the subsurface lithologic and density distribution given the observed gravity data  $y$ . This quantity is proportional (up to a normalization constant  $c$ ) to the product of the two prior pdfs,  $\pi_p(\mathbf{m}_{\text{pri}})$ , which considers the primary lithological subspace, and  $\pi_{s|p}(\mathbf{m}_{\text{sec}} | \mathbf{m}_{\text{pri}})$ , a conditional pdf describing the dependence of the bulk density on the lithology, and a likelihood function,  $L(y | \mathbf{m}_{\text{sec}})$ , which quantifies probabilistically the misfit between the gravity potential field calculated from the joint model and the observed gravity data (see Eq. 5).

### Specification of the prior

The aim of Bayesian inversion of gravity data is to infer the subsurface lithology and density distribution in light of gravity data and the prior geologic understanding of the system. Three types of geologic constraints are used to ensure that posterior results retain geologic meaning from the reference prior geologic model (Intrepid Geophysics, 2017a, 2017b):

- The preservation of vertical stratigraphic order, forcing model realizations to respect the vertical sequence of the stratigraphic units as specified in the reference prior geologic model.

- A commonality constraint describing the expected similarity between the voxel lithology in the reference prior geologic model and model proposals.
- A shape ratio constraint describing the expected roughness of the boundaries between the lithologic units.

In addition, the inversion process is not allowed to change the lithology of voxels that intersect the surface (the surface geologic map is unchanged by the inversion process). Unless otherwise noted, the lithology of voxels in the subsurface are not held constant during the inversion process. Thus, differential geological data quality is not considered and all voxels are equally uncertain. This contrasts with some other probabilistic geologic modeling schemes (De La Varga et al. 2019; Wellmann et al. 2017), which directly invert for the contact point and orientation measurements controlling the implicit interpolation.

The inversion runs performed in this study are described in Table 1. The first suite of runs consists of 'prior-only' inversion tests, where 500,000 samples are generated from the prior distribution without consideration of geophysical likelihoods to illustrate the prior probability space implied by the reference prior geologic model and the assumed geologic constraints. Case 0 explores the prior probability space of the model in the absence of any geologic constraints, and Case 1a–c and 1d–f explore the effect of the commonality and shape ratio constraints, respectively. Since the inversion scheme generates proposals by proposing changes to the reference prior model one voxel at a time, the reference prior model exerts an influence on the probability space implied by the

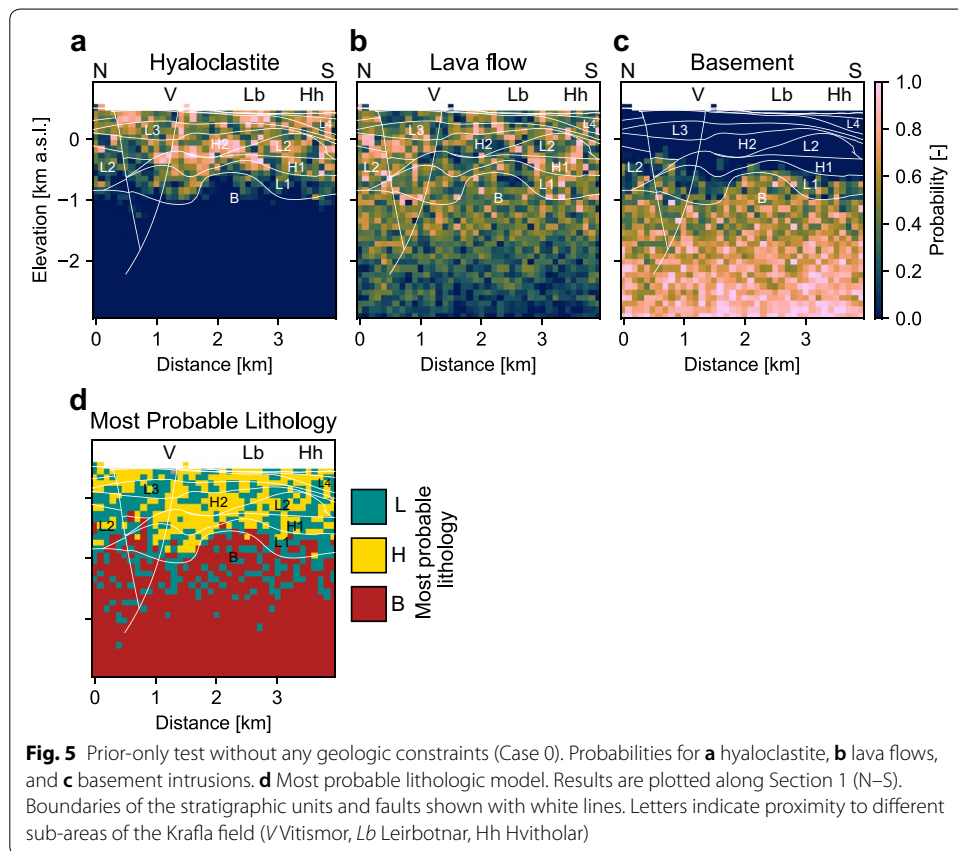
**Table 1 Inversion runs**

Name	PVSR	Commonality constraint	Shape ratio	Probability lithologic changes (%)	Altered hyaloclastites	Rhyolitic intrusion	Consider geophysical likelihood	Gravity measurement error
Case 0	No	No	No	100	No	No	No	–
Case 1a	Yes	Loose	No	100	No	No	No	–
Case 1b	Yes	Moderate	No	100	No	No	No	–
Case 1c	Yes	Tight	No	100	No	No	No	–
Case 1d	Yes	No	Smoother	100	No	No	No	–
Case 1e	Yes	No	Similar	100	No	No	No	–
Case 1f	Yes	No	Rougher	100	No	No	No	–
Case 2a	Yes	No	No	0	No	No	Yes	0.1
Case 2b	Yes	No	No	50	No	No	Yes	0.1
Case 2c	Yes	No	No	100	No	No	Yes	0.1
Case 3a	Yes	Loose	No	50	No	No	Yes	0.1
Case 3b	Yes	Moderate	No	50	No	No	Yes	0.1
Case 3c	Yes	Tight	No	50	No	No	Yes	0.1
Case 3d	Yes	No	Smoother	50	No	No	Yes	0.1
Case 3e	Yes	No	Similar	50	No	No	Yes	0.1
Case 3f	Yes	No	Rougher	50	No	No	Yes	0.1
Case 4a	Yes	Moderate	Rougher	50	Yes	No	Yes	0.1
Case 4b	Yes	Moderate	Rougher	50	Yes	No	Yes	0.5
Case 5a	Yes	Moderate	Rougher	50	Yes	No	Yes	0.1
Case 5b	Yes	Moderate	Rougher	50	Yes	Yes	Yes	0.1

PVSR Preservation of vertical stratigraphic relationships from reference prior model

reference prior model even in the absence of any geologic constraints (Case 0, Fig. 5). The incremental repositioning of boundaries explains why even though preservation of vertical stratigraphic relationships of the reference prior geologic model are not enforced in Case 0, hyaloclastites have a higher probability of occurring at shallower depth (Fig. 5a), lava flows at intermediate depths (Fig. 5b), and basement intrusions at depths >1 km b.s.l (Fig. 5c), broadly consistent with the structure of the reference prior model. However, the lateral continuity of the hyaloclastite and lava flow units described by the reference prior model is lost in the absence of geologic constraints (Fig. 5d), contradicting geologic evidence of the layered structure of lava flows and hyaloclastites (Walker 1971). While the assumption of the preservation of vertical stratigraphic relationships from the reference prior model in accepted model realizations implies that stratigraphic units can not be created (e.g., basement intrusions in between hyaloclastite and lava flow units), they can be destroyed as the boundaries of over- and underlying stratigraphic units shift down- or upward, respectively.

In addition to assuming the preservation of vertical stratigraphic relationships, we quantify beliefs about the uncertainty of the reference prior model using the commonality and shape ratio constraints. The commonality constraint describes the probability of a proposed model as a function of how closely the proposed distribution of lithologies resembles the reference prior model. The pdf describing the probability of



a model configuration as a function of commonality misfit is given by a Weibull distribution, which for a scale parameter  $\lambda > 0$  and shape parameter  $\kappa > 0$  is given as

$$\pi(x|\lambda, \kappa) = \left(\frac{\kappa}{\lambda}\right) \left(\frac{x}{\lambda}\right)^{\kappa-1} \exp\left(-\left(\frac{x}{\lambda}\right)^\kappa\right), \quad (3)$$

where  $x$  is the commonality misfit function, defined as

$$x = \frac{1}{\frac{\text{Same}(j)}{\text{Ref}(j)}} - 1 \quad (4)$$

where  $j$  is the index over the voxels,  $\text{Ref}(j)$  is the set of voxels in the reference geological model, and  $\text{Same}(j)$  is the number of voxels in the intersection between the set of voxels in the current model and the reference model. The expected value of a Weibull distribution is given by  $E = \lambda\Gamma(1 + \frac{1}{\kappa})$ , where  $\Gamma$  is the gamma function. Thus, since we assume  $\kappa = 1$  (in which case the Weibull distribution reduces to an exponential distribution with mean  $\lambda$ ), assumption of a scale parameter of 0.5 (moderate commonality constraint) implies an expected 67% overlap between the set of voxels defined for a particular stratigraphic unit in the reference model and those voxels in model realizations. A scale parameter of 0.05 implies a 95% overlap (tight commonality constraint), and a scale parameter of 5 implies a 17% overlap.

The shape ratio constraint is used to constrain the roughness of the lithologic units. For a particular formation, shape is given by the ratio of the square root to the cube root of the volume, and shape ratio is the ratio of the shape of the proposed model formation divided by the shape of the formation in the reference model. The probability of a proposed model configuration as a function of shape ratio is given by a log normal distribution. In this study, we vary the mean of the log-normal distribution to 0.8, 1, or 1.2, corresponding to an expectation of 20% smoother, similar, or 20% rougher lithologic units, as quantified by the shape ratio, and set the standard deviation to 0.05.

'Prior-only' tests were carried out to assess the effect of varying the strength of the commonality and shape ratio constraint on the prior probability space implied by the reference prior geologic model. Figure 6a–c shows the prior probability of hyaloclastite along Section 1 for a tight, moderate or loose commonality constraint, respectively. The spatial distribution of prior probability more closely resembles the reference prior model when there is a tight commonality constraint (Fig. 6a). As the commonality constraint is loosened (Fig. 6b, c), the zones of intermediate probability along the edges of the hyaloclastite units become more diffuse. Figure 6d–f shows similar results for a smoother, similar or rougher shape ratio constraint. If model realizations with smoother lithologic boundaries compared to the reference model are favored (Fig. 6d), the boundaries between the hyaloclastite units are flat. Even if model realizations with rougher lithologic boundaries are favored, the boundaries between the high hyaloclastite probability areas are less jagged than the loose or moderate commonality constraint and no shape constraint. Thus, the commonality and shape ratio constraints allow expected beliefs about the uncertainty of the location of the lithologic units and the roughness of the boundaries to be expressed.

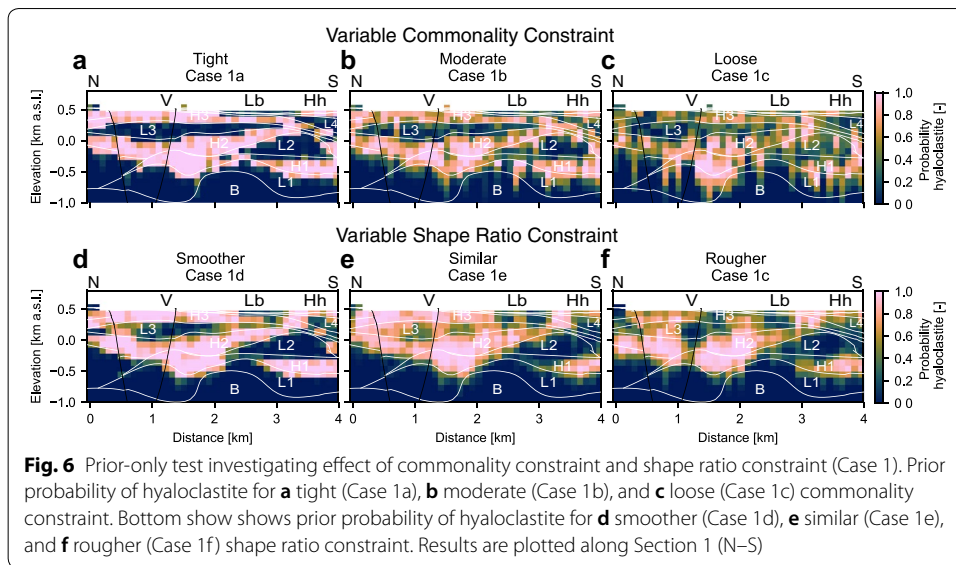


**Fig. 6** Prior-only test investigating effect of commonality constraint and shape ratio constraint (Case 1). Prior probability of hyaloclastite for **a** tight (Case 1a), **b** moderate (Case 1b), and **c** loose (Case 1c) commonality constraint. Bottom show shows prior probability of hyaloclastite for **d** smoother (Case 1d), **e** similar (Case 1e), and **f** rougher (Case 1f) shape ratio constraint. Results are plotted along Section 1 (N–S)

### Stochastic inversion methodology

A Markov chain records a pseudo-random walk in a model space, with a model outcome at each step  $t$  of the walk until a final step  $T$ . A Markov chain is ergodic to a pdf  $\pi(\mathbf{m})$  if the set of model outcomes from the chain  $S^T = \{\mathbf{m}^1, \mathbf{m}^2, \dots, \mathbf{m}^T\}$  converges to  $\pi(\mathbf{m})$  as the number of steps increases. To estimate the posterior probability density, three Markov chains corresponding to the three terms in Eq. 3 are generated (Bosch 1999; Bosch et al. 2001):

- A primary chain considering the lithological prior.
- A prior chain considering both the lithological and petrophysical prior information.
- A posterior chain, which modifies the prior chain to generate joint models of the lithology and density distribution constrained by the geophysical likelihood.

For the primary chain, a Metropolis sampling rule (Metropolis et al. 1953) considering the probability of a proposed model configuration as a function of commonality misfit and/or shape ratio was used to generate a chain ergodic to  $\pi(\mathbf{m}_{pri})$ . The prior chain samples from a joint pdf using an outcome from the primary chain (a marginal pdf) to sample from the conditional pdf  $\pi_{s|p}(\mathbf{m}_{sec} | \mathbf{m}_{pri})$ . For the posterior chain, the Metropolis test considers the geophysical likelihood to generate a Markov chain ergodic to the posterior probability density  $\pi(\mathbf{m}_{sec}, \mathbf{m}_{pri} | y)$ , respectively, similar to the framework described by Mosegaard and Tarantola (1995).

The likelihood of a proposed model is calculated based on the misfit between the simulated gravity response of a proposed geologic model and the observed data. For details on how the vertical component of the gravitational field is calculated based on a combination of the contributions of all the voxel cells as a function of their positions and densities, see Li and Oldenburg (1998). As described by Guillen et al. (2008), the likelihood is given by

$$L(y | \mathbf{m}_{sec}) = k \exp(-S(y | \mathbf{m}_{sec})/\sigma^2), \tag{5}$$

where  $k$  is a normalization factor, and  $\sigma^2$  is the variance of the data (i.e., measurement error), and  $S(y | \mathbf{m}_{sec})$  the L2-norm misfit with the gravity field, calculated as

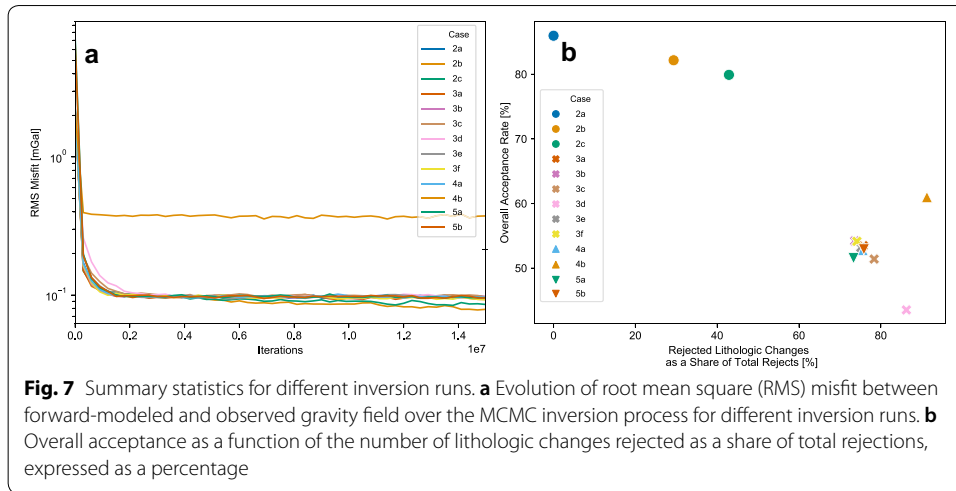
$$S(y | \mathbf{m}_{\text{sec}}) = \frac{1}{2} \sum_{l=1}^N [g^l(\mathbf{m}_{\text{sec}}) - y^l]^2, \quad (6)$$

where  $g^l(\mathbf{m}_{\text{sec}})$  represents the modeled gravity field at the point of observation  $l$  while  $y^l$  represents the measurement of the gravity field at the same point. Based on analysis of repeated gravity measurements at different stations and uncertainty of 30 cm in the elevation measurements, the measurement error is estimated to be 0.1 mGal. However, this is likely an underestimation of the uncertainty of the gravity data, particularly in locations with a low spatial density of measurement stations, and we vary the measurement error to 0.5 mGal (Case 4b).

According to the Metropolis rule, if the likelihood of a proposed model based on the calculated gravity response has a lower misfit with the measured data (higher likelihood) compared to the previous model, the proposed model is accepted and stored for determination of the posterior statistics. Otherwise, a proposed model is accepted with a probability given by the ratio of its probability with the previous model. For all of the inversion runs considering geophysical likelihood (Cases 2–5), fifteen million iterations were carried out. We assess convergence of the Markov chain on the basis of the calculated misfit between the forward modeled gravity field and observed data (calculated as root mean square, RMS, Eq. 6). The value at which the RMS misfit stabilizes reflects the assumed measurement error of the gravity data. For inversion runs assuming a measurement error of 0.1 mGal, we store models for calculation of posterior statistics after the inversion processed reduces RMS misfit to less than 0.15 mGal, which usually occurs within 1,000,000–1,500,000 iterations (Fig. 7a). Model realizations calculated before this misfit value has been reached are discarded as burn-in. Case 4b assumes higher measurement error (0.5 mGal), and as a result the inversion process stabilizes the misfit at higher value ( $\sim 0.4$ ).

Proposed model configurations are generated by changing the density or changing the lithology (and thereby, the bulk density) of randomly selected voxels. Thus, one of the key parameters controlling the inversion process is the probability that changes to lithology are proposed. If the probability of lithologic changes is set to 0 (Case 2a), the lithologic structure of the reference prior model serves as a hard constraint on the geometry of the stratigraphic units in model realizations, and only the density of each voxel is changed according to the specified pdfs for each lithotype. In contrast, maximum variability in lithologic structure is attained by setting the probability of lithologic changes to 100%, as is done for the ‘prior-only’ tests.

A density-only inversion (Case 2a) has a high acceptance rate ( $\sim 85\%$ ), and increasing the fraction of proposed lithologic changes slightly decreases the overall acceptance rate (Fig. 7b). However, if commonality and/or shape ratio constraints are also assumed (Cases 3–5), more models with proposed lithologic changes are rejected, and the overall acceptance rate declines to 50–55%. The acceptance rate is somewhat higher if there is a higher assumed measurement error (Cases 4b and 4c), and lower if a smoother shape ratio constraint is assumed (Case 3d). The high rate at which proposed geologic changes are rejected indicates a need for a long chain to adequately explore the lithology probability space. Link and Eaton (2012) suggest that a better



approximation of posterior statistics for a chain exhibiting autocorrelation can be obtained by simply making the chain  $N$  times longer, rather than thinning the chain by only considering every  $N$ th sample. This accounts for the length of the MCMC chain in Cases 2–5 (15,000,000 samples).

The uncertainty of model predictions depends on the strength of the geologic constraints imposed on the probabilistic inversions. For a discrete variable such as litho-type, the uncertainty of probabilistic geologic models can be quantified by the information entropy metric. For each voxel, the information entropy is given by (Shannon 1948; Wellmann and Regenauer-Lieb 2012)

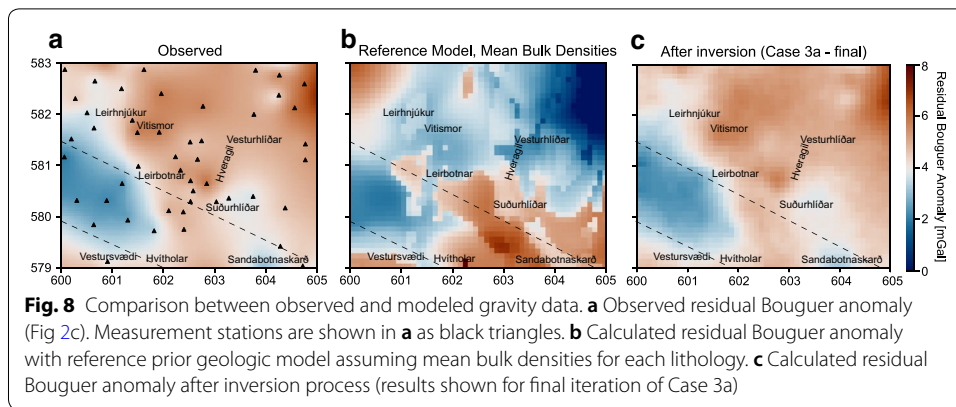
$$H(x) = - \sum_{m=1}^M \pi_m(x) \log(\pi_m(x)), \tag{7}$$

where  $x$  denotes the location of the voxel and  $M$  the number of possible exclusive members (in this case, lithologies) the subregion can contain. The minimum entropy is 0, which indicates that a specific lithology has a probability 1 and that of all others is 0. The maximum entropy depends on the number of possible outcomes, and is found where the different possible lithologies are equally probable. The uncertainty of continuous variables such as bulk density can be characterized in terms of standard deviation.

## Results

We present results for posterior probability distributions and uncertainty quantification metrics along the three cross sections shown in Fig. 3 (Section 1, a N–S section going through Vitismor, Leirbotnar, and ending north of Hvítholar; Section 2, a SW–NE section going through Vestursvaeði, Leirbotnar, Hveragil and Vesturhlíðar; and Section 3, a NW–SE section going through Leirhnjúkur, Vitismor, Leirbotnar, Hveragil and Suðurhlíðar). We use perceptually uniform color maps to present the model results to avoid visual distortion of the data (Crameri 2018).



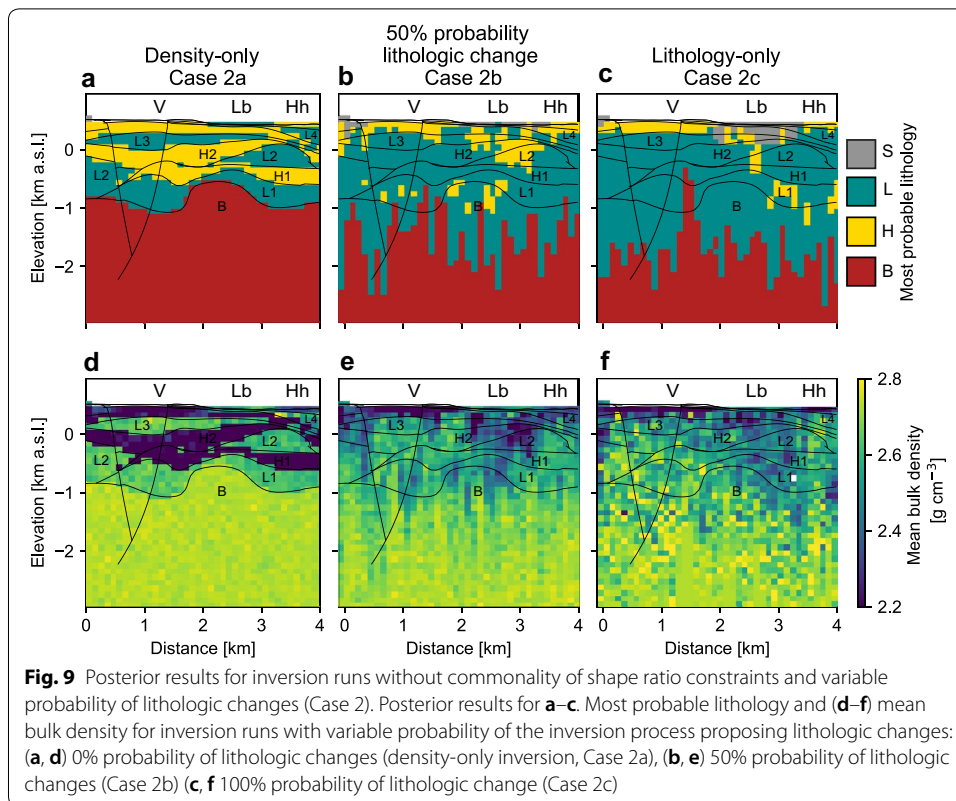


### Comparison between observed and forward modeled gravity field

The inversion process reduces misfit between the forward modeled gravity potential field and the measured data. The range of the residual Bouguer anomaly calculated using the reference prior model and assuming mean bulk densities for each rock type (Fig. 8b) overlaps with the observed data (Fig. 8a), and predicts lower gravity values (2–4 mGal) in the SW between Leirbotnar and Vestursvæði bordered by a gravity high to the W or Sudurhlidur, similar to the observed data set. However, other anomalies seen in the observed data are not resolved, such as the high gravity anomaly in the NE, where a gravity low is calculated by the reference model. After the inversion process, there is a close correspondence between the gravity field calculated for the changed model and the measured data (Fig. 8c), with the absolute misfit less than 0.3 mGal. Note that Fig. 8 shows results at the end of Case 3a; the gravity field calculated varies slightly depending on the step in the inversion process and the run configuration. However, as shown in Fig. 7a, the absolute misfit values during the inversion process are nearly constant depending on the assumed measurement error of the gravity data.

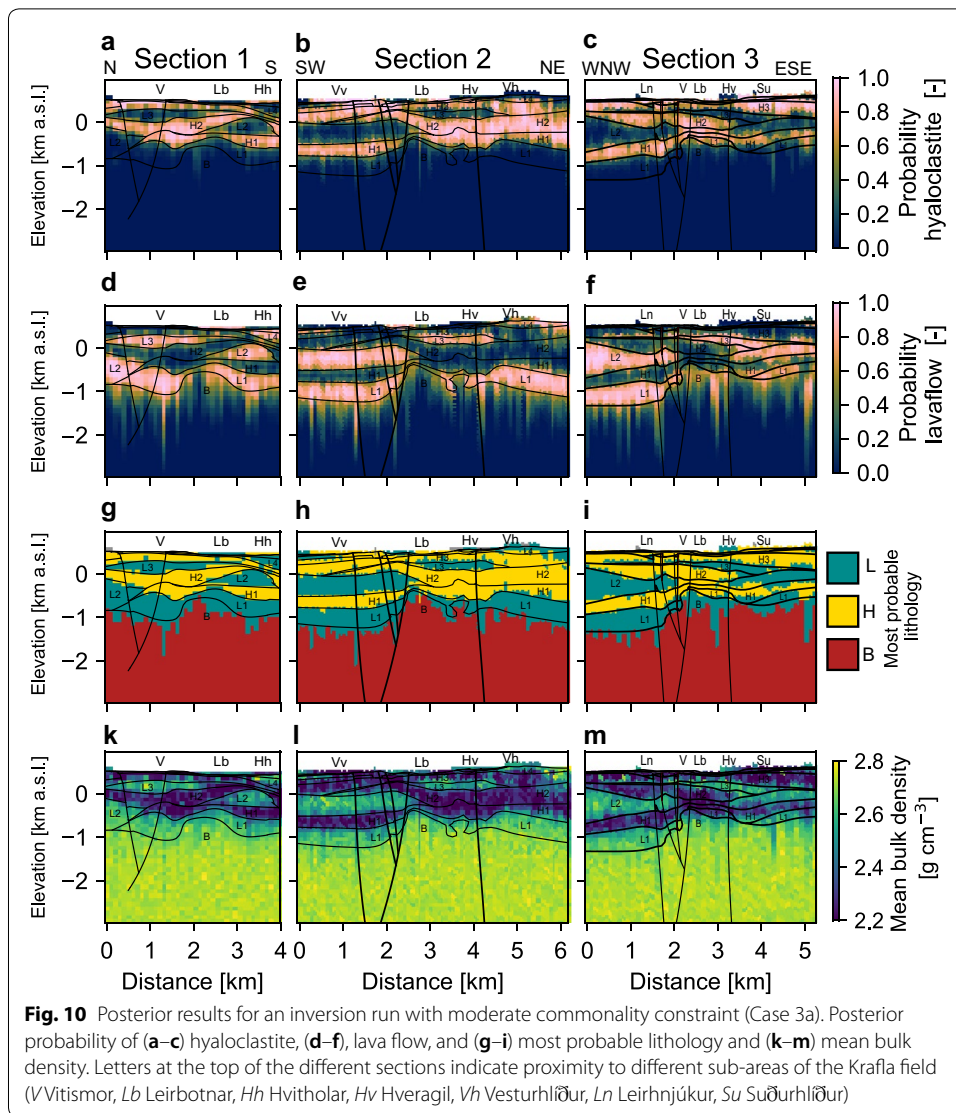
### Litho-constrained inversion

The geologic constraints imposed on the inversion scheme determine the extent to which geologic prior information is reflected in posterior results. For a density-only inversion (Case 2a), the reference prior model serves as a hard constraint on model realizations (Fig. 9a). However, if the inversion scheme is allowed to propose changes to the lithologic structure of the reference prior model without the use of commonality and/or shape ratio constraints (Case 2b and 2c), the lithologic structure of the reference prior model is lost in the posterior results. The most probable lithologic structure calculated by these inversion runs strongly differs from the reference prior model, most notably by predicting deeper basement intrusions, more extensive lava flows, and relatively minor hyaloclastites (Fig. 9b, c). Whereas for a density-only inversion the hyaloclastite units constitute distinct domains with low bulk density ( $\sim 2.2 \text{ g cm}^{-3}$ ) within the higher density lava flows ( $\sim 2.6 \text{ g cm}^{-3}$ ), there is a smearing out of low density zones in the upper 2 km if lithologic changes are proposed to the reference prior model in the absence of other geologic constraints such as the commonality and/or shape constraint (Fig. 9d–f).



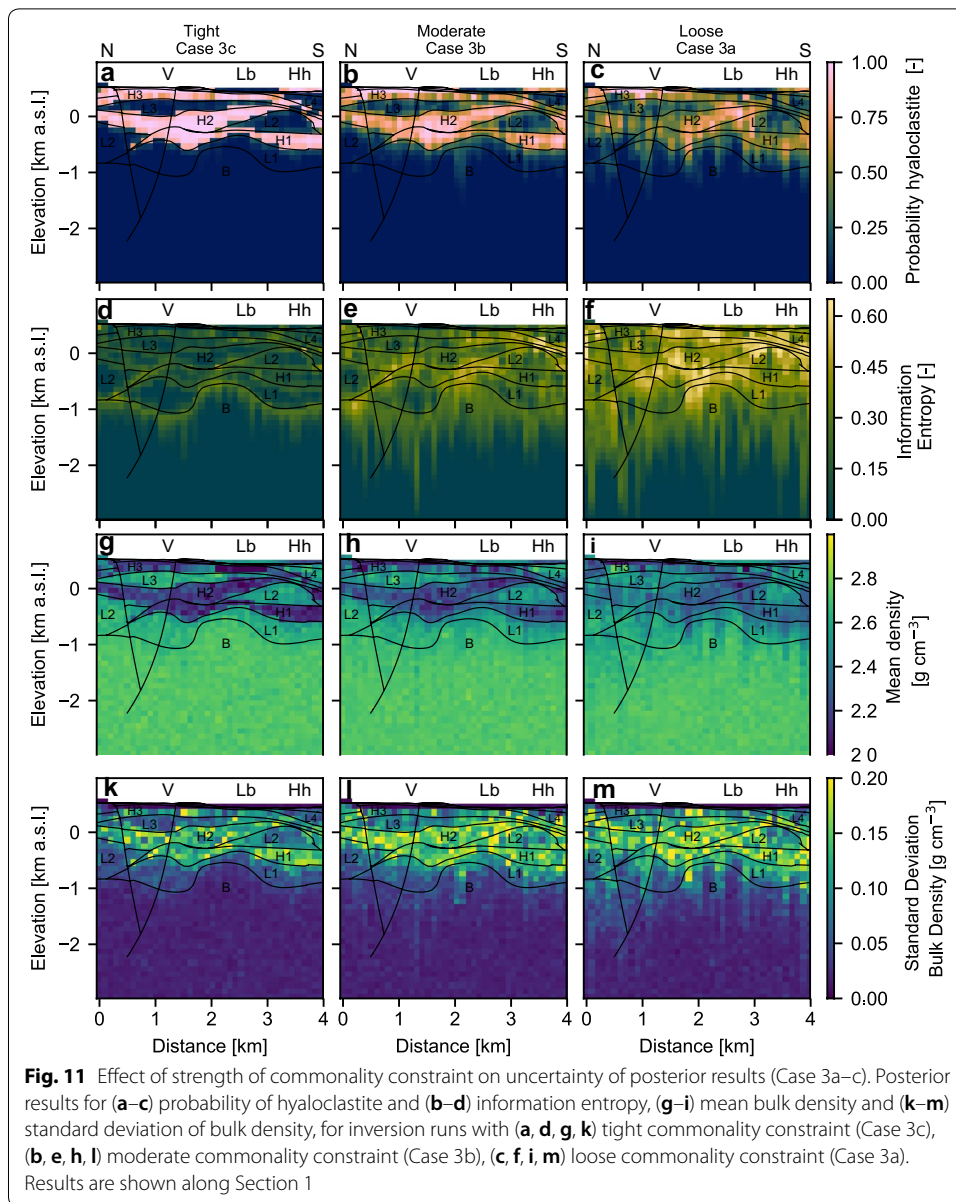
A moderate commonality constraint causes the inversion process to retain the lithologic structure of the reference prior model in the posterior results while also allowing some significant differences (Case 3a, Fig. 10). For example, the regions of high posterior probability for hyaloclastite (Fig. 10a–c) and lava flow (Fig. 10d–f) coincide with the boundaries of the hyaloclastite and lava flow units described by the reference prior model. However, there is also a high probability of lava flow occurring beneath the lowermost lava flow unit L1, particularly beneath Vitismor, Hveragil and Leirbotnar (Fig. 10d–f). Accordingly, the most probable lithologic model (Fig. 10g–i) predicts a 0.1–0.2 km greater depth to basement throughout much of the model domain, with this discrepancy extending up to 1 km in the area, where the basement rock extends to ~ 1–1.5 km depth between Vitismor and Hveragil according to the reference prior model.

Due to the strong similarity between the lithologic structure of the posterior and the reference prior model, the calculated density structure assuming a moderate commonality constraint (Fig. 10k–m) is similar to that calculated by a density-only inversion, with strong contrasts preserved between the lithologic units. Hyaloclastites show a low mean bulk density (~ 2.2 g cm<sup>-3</sup>) compared to the higher density lava flows (~ 2.6 g cm<sup>-3</sup>) and basement intrusions (~ 2.8 g cm<sup>-3</sup>). Comparing the posterior results for bulk density to lithology on Section 3 (Fig. 10m), it can be seen that the relatively low mean bulk density (2.5–2.6 g cm<sup>-3</sup>) near the top of the basement intrusions beneath Leirbotnar reflects the high posterior probability of lava flows occurring at such depths in this area.



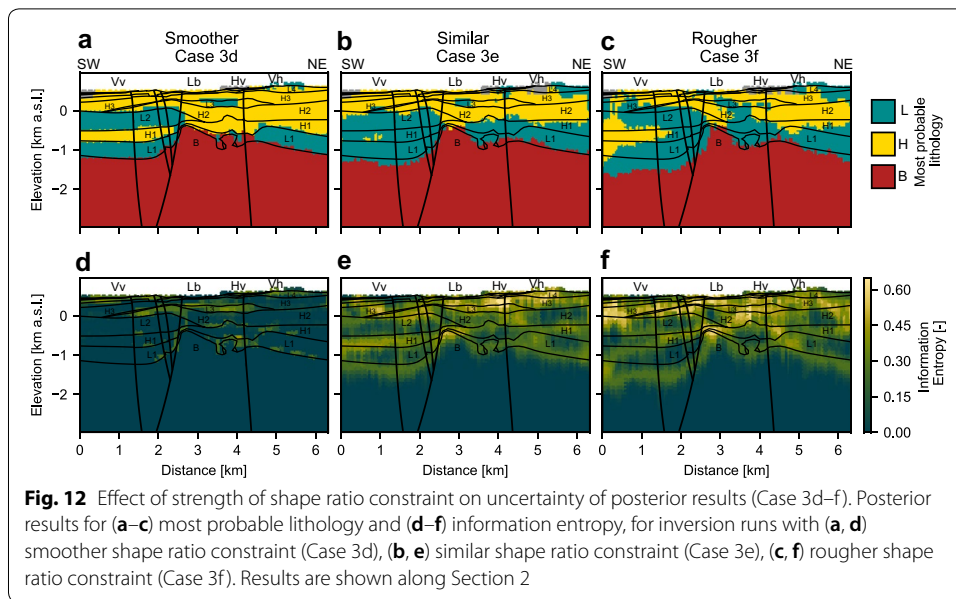
### The effect of variable commonality and shape ratio constraint

The level of uncertainty of the reference prior geologic model can be quantified by the strength of the commonality and shape ratio constraints. Figure 11 considers the effect of commonality constraint on the uncertainty of posterior results. If a tight commonality constraint is assumed, hyaloclastite has a high probability of occurring within the hyaloclastite layers described the reference prior model (Fig. 11a), similar to a density-only inversion. If the strength of the commonality constraint is lowered, voxel hyaloclastite probabilities become increasingly lower and more widely spread through the upper 1.5 km (Fig. 11b, c). The increasing uncertainty of the posterior as the commonality constraint is loosened is revealed by the higher information entropy (Fig. 11d–f), particularly along the lithologic boundaries and in areas with intermediate hyaloclastite probabilities. Accordingly, the low mean bulk density of the hyaloclastite units at shallow depths become less distinct as the strength of the commonality constraint is



reduced (Fig. 11j–l), and the standard deviation of density at shallow depths increases (Fig. 11m–o).

The shape ratio constraint allows the roughness of the lithologic units to be controlled. However, the size and locations of the lithologic units can be different if a shape ratio constraint is used without a commonality constraint (Fig. 12). Figure 12a shows that the lithologic structure of the posterior is similar to the reference model if the lithologic units are assumed to be smoother than the reference prior model, indicating that the number of accepted lithologic changes is relatively low (Fig. 7b). If the lithologic units are assumed to have a similar roughness as given by the reference prior model (Fig. 12b), there are significant differences in the size and locations of lithologic units according to the most probable lithologic model compared to the reference prior model, and the lowermost hyaloclastite unit (H1) is not present. If lithologic units are assumed to be



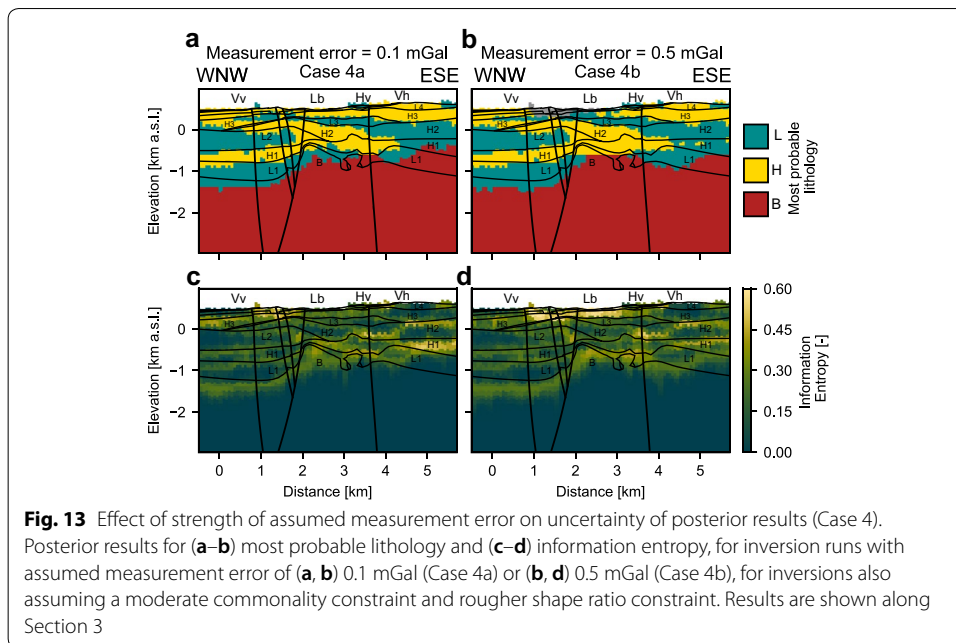
rougher than the reference prior model, the boundaries between the lithologic units become more jagged, as indicated by an increase in the contrast between the depth of the basement in Vestursvaedi and Leirbotnar (Fig. 12c). Similar to the commonality constraint, the information entropy increases as the shape ratio constraint favors increasingly rough lithologic boundaries (Fig. 12e, f).

**The effect of assumed measurement error**

In addition to the uncertainty of the reference prior geologic model, there is uncertainty in the gravity data stemming from measurement error and limited spatial coverage. Figure 13 shows how increasing the uncertainty of the gravity data from 0.1 mGal (Case 4a) to 0.5 mGal (Case 4b), as specified by the measurement error ( $\sigma^2$  in Eq. 6), affects the posterior results for inversion runs with a moderate commonality constraint and a rougher shape ratio constraint. The posterior lithologic structures generally appears to depend little on the assumed measurement error (Fig. 13a–b). However, one notable difference is that hyaloclastites have a higher probability at 1–1.5 km depth beneath Leirbotnar if a high measurement error is assumed (Fig. 13b). In this area, information entropy is up to 0.45, indicating a high uncertainty, even if the measurement error is assumed to be low (Fig. 13c–d).

**Changing the prior properties and lithologic structure**

The posterior distributions of bulk density and lithology change if higher density, altered hyaloclastites or a low density rhyolytic intrusion beneath the center of the caldera are considered in the reference prior model. On the left of Fig. 14a, results for most probable lithology and mean bulk density are shown along Section 3 for the scenario with unaltered hyaloclastites, a moderate commonality constraint, a rougher shape ratio constraint, and a low measurement error (Case 4a). Changing the prior pdf for the bulk density of hyaloclastite to account for the effects of alteration (Case 5a) causes the

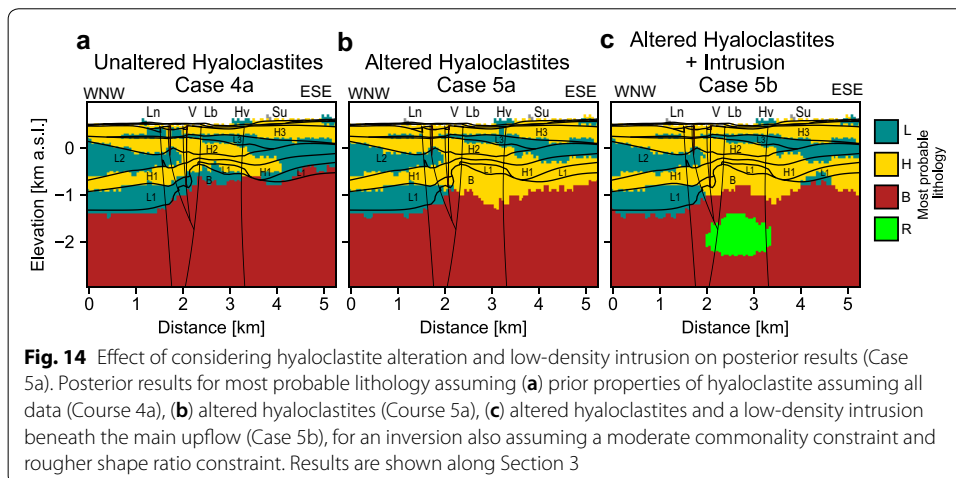


hyaloclastite at the top of the basement beneath Leirbotnar to expand to greater depths and towards the ESE (Fig. 14c). If the reference prior model also considers the presence of an oblate rhyolitic intrusion at 2 km depth beneath Vitismor and Leirbotnar (Case 5b), with a horizontal and vertical axes lengths of 1.5 and 1 km, respectively, and a low density of  $2.3 \pm 0.1 \text{ g cm}^{-3}$  (Bagdassarov and Dingwell 1994; Ochs and Lange 1999), the extent of the hyaloclastites at depth above the intrusion decreases compared to Case 5a.

## Discussion

### The uncertainty of the prior

Bayesian inversion of gravimetric data enables the use of subjective prior information to eliminate unreasonable models that may potentially fit the data. One of the challenges



of such inversion schemes is to specify the uncertainty of geologic prior information in such a way that both honors the geologic complexity and allows the inversion scheme to adequately explore the range of possible models that may be consistent with the data. Some approaches to probabilistic geologic modeling specify the uncertainty of the geologic model in terms of prior pdfs for the contact point and orientation measurements (De La Varga et al. 2019; Wellmann et al. 2017). In this study, the reference prior geologic model represents an interpretation of the subsurface lithologic structure. Therefore, we specify the uncertainty of this prior model using probabilistic constraints on the expected location, size and shape of lithologic units (commonality and shape ratio constraints), and invert for voxel lithology and bulk density, rather than contact point and orientation measurements.

Our results document the strong control the uncertainty of the geologic prior exerts on the posterior results obtained by litho-constrained, Bayesian inversion of gravity data. Without constraints on commonality or shape ratio, the posterior lithologic structure shows little similarity to the prior, even if the vertical stratigraphic relationships from the reference model are respected (Fig. 9b, c). In contrast, if a tight commonality constraint (Fig. 11a) or smoother shape ratio constraint (Fig. 13a) is imposed, the posterior lithologic structure closely resembles the reference prior model, similar to a density-only inversion (Fig. 9a). We consider that the assumption of a moderate commonality constraint and rougher shape ratio constraint (Cases 4 and 5) respects the prior information while also allowing a degree of divergence between the prior and posterior in zones of high uncertainty, where the prior model may need to be revised.

Posterior results deviate from the reference prior model most notably beneath Leirbotnar, Vitismor and Hveragil, where the inversion results predict hyaloclastites between 1–1.5 km depth and basement intrusions restricted to >2 km depth (Fig. 14). The hyaloclastites are predicted to extend laterally and to greater depths if high measurement error of the gravity data is assumed (Fig. 13b), or if the prior pdfs for the bulk density of the hyaloclastite units are set to higher, more realistic values, reflecting the effects of high-temperature rock alteration (Fig. 14b). The predicted extent of the hyaloclastites decreases slightly if a low-density rhyolitic intrusion at depth beneath this area (Fig. 14c). As there is direct evidence of shallow basement intrusion at depths > 1 km b.s.l. in this area from drill cuttings (Mortensen et al. 2014; Weisenberger et al. 2015), we consider that the prediction of deep hyaloclastites in this area is erroneous. This reveals one of the disadvantages of an approach that assumes all voxels are equally uncertain, as the most uncertain areas predicted by the probabilistic inversion scheme may in fact be constrained by available hard data. In addition to the uncertainty of the geologic model, the uncertainty of hyaloclastite bulk density plays a large role in controlling model results in the area of the discrepancy. In calculation of the bulk density pdfs, we assume a uniform fluid density of  $0.8 \text{ g cm}^{-3}$ . However, circulating water expands to low densities ( $< 0.4 \text{ g cm}^{-3}$ ) as it is heated near subsurface intrusions (Scott et al. 2015), and vapor-rich boiling zones extending to up to 2 km depth may develop within upflow zones (Scott et al. 2016). Since the area between Leirbotnar and Hveragil coincides with the main upflow zone of Krafla system (Pope et al. 2016), considering a more realistic distribution of fluid density would likely reduce the subsurface bulk density in this area and potentially reduce the discrepancy.

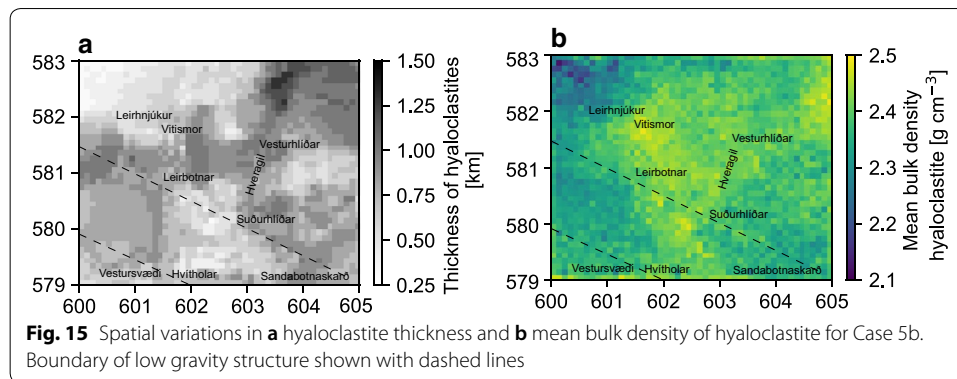
### Implications for the Krafla system

The positive gravity anomaly associated with the Krafla caldera (Fig. 2) has been seen in other Icelandic volcanic systems (Gudmundsson and Milsom 1997; Gudmundsson and Högnadóttir 2007), and is typical of basaltic volcanoes generally (Williams and Finn 1985). Previous gravity studies of volcanoes in the Northern Volcanic Zone of Iceland have linked the gravity highs to dense intrusions in the upper crust (de Zeeuw-van Dalfsen et al. 2006; Rymer and Tryggvason 1993; Rymer et al. 1998). However, Árnason et al. (2007) suggested that the local gravity highs at and inside the caldera rim at Krafla are not indicative of intrusions, as such steep gradients could only result from density contrasts at shallow depths (< 1 km). Instead, Árnason et al. (2007) suggested that the gravity field mainly reflects variations in hyaloclastite thickness, and inferred the existence of a buried inner caldera, the focus of this study, containing thicker hyaloclastite and deeper basement than the outer caldera. Supported by early borehole data from showing deeper basement and thicker hyaloclastite in Hvitholar in the south (Ármansson et al. 1987), the WNW–ESE oriented gravity low transecting the caldera was posited to represent a transform graben, containing thicker sequences of hyaloclastite (Árnason et al. 2007).

In this study, we suggest that gravity field at Krafla also reflects systematic differences in the spatial distribution of hyaloclastite density resulting from variable alteration. Fresh, unaltered hyaloclastite can show extremely high initial porosity and low bulk density (Fig. 4). However, hyaloclastite is weak and undergoes inelastic compaction at relatively low effective pressures (Eggertsson et al. 2018), leading to porosity destruction and density increase (Frolova 2008). While lava flows or basement intrusions will undergo porosity closure at relatively small degrees of alteration (Thien et al. 2015), the high initial porosity of hyaloclastites allows near or complete alteration. Altered hyaloclastites show lower porosity and higher grain density (Fig. 4), particularly if subject to high-temperature alteration in the chlorite, chlorite–epidote, or epidote–actinolite facies. The susceptibility of hyaloclastite to alteration suggests that a region of unaltered hyaloclastite within a larger high-temperature geothermal system may be detectable as a gravity low. Due to the processes of compaction and alteration, we consider the values from the tightly-constrained inversions to be an underestimation of hyaloclastite density. As most of the data shown in Fig. 4 originate from the samples obtained from exhumed geothermal systems at the surface or from shallow cores (< 0.5 km depth), this data may be poorly representative of hyaloclastite at greater depths.

Our models predict lower hyaloclastite densities within the transverse low gravity structure. Figure 15 shows a map view of the thickness of hyaloclastites according to the most probable model (Fig. 15a) and mean bulk density of hyaloclastites, calculated by averaging the mean density of all voxels in a vertical column with hyaloclastite as the most probable lithology (Fig. 15b) for Case 5b. Hyaloclastite thickness is predicted greatest in the center part of the field, near Leirbotnar (Fig. 15a). While these hyaloclastites are predicted to be relatively high density, lower hyaloclastite density is predicted in the NW of the caldera, and within the WNW–ESE oriented gravity low, particularly in the southwest. We suggest that the low hyaloclastite density within the WNW–ESE oriented gravity low could be an indication of a lack of high-temperature alteration in this area. This is also suggested by the alteration data, which suggests an increase in the depth of





the smectite–zeolite zone in Sandabotnaskard (Weisenberger et al. 2015), as well as the resistivity structure of the system, which shows that the shallow low-resistivity cap rock does not extend in the area of the WNW–ESE-oriented gravity low structure (Gasperi-kova et al. 2015; Rosenkjaer et al. 2015).

Transform structures with a WNW–ESE-orientation in the Northern Volcanic Zone develop as a result of the westward step-over in the rift that occurs north of Iceland. The dextral WNW–ESE-oriented Husavik-Flatey-Fault is believed to act a conduit for upflow in the Theistareykir system north of Krafla (Khodayar et al. 2018). At Krafla, the basaltic dikes and sills that make up the main heat sources are believed to originate from the WNW–ESE structure and incline towards the north (Weisenberger et al. 2015), resulting in the main upflow being located beneath Leirbotnar and Sudurhlíður. Potentially, a buried WNW–ESE-oriented fault could divert fluids outflowing southwards away from the main upflow upwards. Such fault barriers to flow are commonly observed in geothermal systems (Cumming 2016). This could explain the near-WNW–ESE alignment of hot springs along the southern margin of the central part of the field (Fig. 1). However, note that the gravity low is transected in the middle by a zone with higher gravity with the same orientation as the Hveragil fault. This fault could act a conduit for high temperature fluid to the south, towards Hvíthólar, where few production wells are located but some are productive.

#### Integration of geological, geophysical and hydrological data sets

This study quantitatively links a geologic model developed based on borehole evidence to observed geophysical data by assigning rock properties informed from laboratory studies to the main lithologic units. As previously studies have also found (Fedi and Rapolla 2002), gravity data alone is unable to resolve the thickness, spatial distribution and physical properties of lithologic units in the absence of strong a priori constraints. To improve resolution, joint inversion of gravity data with magnetic, seismic or magnetotelluric (MT) datasets can be performed, assuming structural similarities between the different geophysical domains (Oliver Ocaño et al. 2019; Soyer et al. 2017) or using geologically conditioned petrophysical constraints to link the different domains (Giraud et al. 2017). However, due to the inability to distinguish major rock types solely on the basis of rock properties, geologic conditioning of the inversions in the form of an a priori reference geologic model is essential (Olierook et al. 2019). The electrical resistivity

structure is particularly valuable for imaging geothermal systems (e.g., Cumming 2016), but is more closely linked to alteration than lithology (e.g., Cumming 2016). Therefore, it is essential that these prior models should consider the distribution of alteration zones. Additionally, more data for the bulk resistivity of properties of Icelandic geothermal reservoir rocks (Lévy et al. 2018; Nono et al. 2018) is needed to better constrain the joint prior physical properties pdfs.

The distribution of fluid properties has a significant impact on measured geophysical signals in geothermal systems. Bayesian geophysical inversion schemes that specify heterogeneous fluid properties as part of the prior allow better deciphering of signals from MT inversions (Rosas-Carbajal et al. 2015). Probabilistic fluid flow models of geothermal systems commonly invert for the permeability structure and locations of heat sources, constrained by measured temperature and pressure data (Cui et al. 2011; Maclaren et al. 2018). The distribution of temperature and fluid density from the fluid flow models can constrain the distribution of bulk rock density and resistivity for the gravity and MT inversions, respectively (Garg et al. 2007; Pearson-Grant et al. 2018; Rosas-Carbajal et al. 2015). The development of models that honor all the available geological, geophysical and hydrological data will be challenging, but will provide deeper insight into the relationship between geologic structure and fluid reservoirs in geothermal systems.

## Conclusions

This study presents a suite of probabilistic geologic models of the Krafla geothermal system constrained by measured gravity data. We combine a reference prior geologic model built from borehole data and statistical analysis of rock properties in a Bayesian inference framework to generate a probability distribution describing the distribution of major lithologies and the subsurface density distribution. This study investigates how varying the uncertainty of the prior affects posterior probabilities and uncertainty quantification metrics obtained by probabilistic, litho-constrained inversion of gravity data. For geologically complex systems such as volcano-hosted geothermal systems, knowledge of the structure and properties of the subsurface is not exact. More broadly, even the uncertainty of this knowledge is not very well known. Yet this uncertainty must be specified in the prior, both through the imposed geologic constraints, such as the commonality constraint, and the prior physical property distributions for each lithology. While rock petrophysical properties are measured in the lab may be known with some confidence, measured properties may be systematically biased as a result of the assumption that rock samples collected at the surface are representative of rocks at depth. However, the greater uncertainty lies with the geologic structure.

A main advantage of Bayesian geophysical inversion methods is that subjective prior information can be used to constrain the subsurface structure. However, this study underscores that use of a probabilistic approach to geophysical inversion does not avoid the non-uniqueness problems associated with inversion of potential field data such as gravity data. The observed correspondence between the posterior results and the reference prior geologic model is largely a result of the imposed geologic constraints. That a priori beliefs about the uncertainty of the reference prior model exert such a strong influence on posterior results is seemingly at odds with the philosophy of Bayesian inversion, which aims to condition uncertain beliefs based observed data. However, a

non-informative prior (without the commonality constraint or with a very loose commonality constraint) results in an overly broad, geologically meaningless suite of models that may be consistent with the data. Inversions with different reference prior geologic models and/or prior physical property distributions result in different 'most probable' models, all of which match the observed data. Although posterior results are better thought of in terms of probabilities instead of a most probable model, the point remains that meaningful posterior results depend on having a reliable prior model for geologic structure. Thus, conventional geologic studies (mapping, lithologic analysis, correlation of stratigraphic measurements between boreholes) play an essential role in developing a meaningful prior that can be used for Bayesian inversion of geophysical data. This requirement may limit the utility of Bayesian inference techniques for systems for which only limited geologic data is available.

#### Abbreviations

pdf: probability density function; MT: magneto-telluric; TEM: transient electro-magnetic.

#### Acknowledgements

James Catley, Nataly Castillo Ruiz and Knutur Arnason are acknowledged for fruitful discussions at the early stages of this manuscript. Thanks to Ingvar Thor Magnusson for providing the gravity data and Annette Mortensen for providing the geologic data. Thanks to Hjalti Franzson and ISOR for making the petrophysical data available.

#### Authors' contributions

SWS wrote the manuscript. EJ helped with interpretation of the geologic and gravimetric data. CC performed statistical analyses of the rock properties. All authors contributed to the preparation of the manuscript and the interpretation of the data and model results. MSG led the project. All authors read and approved the final manuscript.

#### Funding

This study was funded by Technical Development Fund of the Research Center of Iceland (RANNÍS—Grant Number 175193-0612 Data Fusion for Geothermal Reservoir Characterization).

#### Availability of data and materials

Regarding the Springer data policy, processed data output from the models developed in this study are shown in Figs. 8, 9, 10, 11, 12, 13, 14, 15, and geologic and gravimetric data can be requested from samuels@ru.is if necessary (the latter data was obtained in processed format from the authors cited in the references). The GeoModeller software platform is proprietary and developed by Intrepid Geophysics (<http://www.geomodeller.com>).

#### Ethics approval and consent to participate

Not applicable.

#### Consent for publication

We confirm that the article nor portions of it have been previously published elsewhere (except as a conference abstract), the manuscript is not under consideration for publication in another journal, and that all authors consent to the publication of the manuscript in *Geothermal Energy*, should the article be accepted upon completion of the review process.

#### Competing interests

The authors declare that they have no competing interests.

#### Author details

<sup>1</sup> Department of Engineering, Reykjavik University, Menntavegur 1, 101 Reykjavik, Iceland. <sup>2</sup> Landsvirkjun, Háaleitisbraut 68, 103 Reykjavik, Iceland. <sup>3</sup> School of Engineering and Natural Sciences, University of Iceland, Reykjavik, Iceland.

Received: 11 January 2019 Accepted: 3 September 2019

Published online: 24 September 2019

#### References

- Abdelfettah Y, Schill E, Kuhn P. Characterization of geothermally relevant structures at the top of crystalline basement in Switzerland by filters and gravity forward modelling. *Geophys J Int.* 2014;199(1):226–41. <https://doi.org/10.1093/gji/ggu255>.
- Altwegg P, Schill E, Abdelfettah Y, Radogna PV, Mauri G. Toward fracture porosity assessment by gravity forward modeling for geothermal exploration (Sankt Gallen, Switzerland). *Geothermics.* 2015;57:26–38. <https://doi.org/10.1016/j.geothermics.2015.05.006>.

- Ármansson H, Gudmundsson Á, Steingrímsson BS. Exploration and development of the Krafla geothermal area. *Jökull*. 1987;37:13–29.
- Árnason K, Vilhjálmsson AM, Björnsdóttir T. A study of the Krafla volcano using gravity, micro-earthquake and MT data. In: Short course II on surface exploration for geothermal resources p. 1–12; 2007.
- Bagdassarov N, Dingwell D. Thermal properties of vesicular rhyolite. *J Volcanol Geotherm Res*. 1994;60(2):179–91. [https://doi.org/10.1016/0377-0273\(94\)90067-1](https://doi.org/10.1016/0377-0273(94)90067-1).
- Björnsson A, Sæmundsson K, Einarsson P, Tryggvason E, Grönvold K. Current rifting episode in north Iceland. *Nature*. 1977;266(5600):318–23. <https://doi.org/10.1038/266318a0>.
- Bosch M. Lithologic tomography: from plural geophysical data to lithology estimation. *J Geophys Res*. 1999;104(B1):749–66. <https://doi.org/10.1029/1998jb900014>.
- Bosch M, Guillen A, Ledru P. Lithologic tomography: an application to geophysical data from the cadomian belt of northern brittany, france. *Tectonophysics*. 2001;331:197–227. [https://doi.org/10.1016/s0040-1951\(01\)00267-0](https://doi.org/10.1016/s0040-1951(01)00267-0).
- Boulangier O, Chouteau M. Constraints in 3D gravity inversion. *Geophys Prospect*. 2001;49(2):265–80. <https://doi.org/10.1046/j.1365-2478.2001.00254.x>.
- Brandsdóttir B, Menke W, Einarsson P, White RS, Staples RK. Färoe-Iceland Ridge Experiment: 2. Crustal structure of the Krafla central volcano. *J Geophys Res*. 1997;102(B4):7867–86.
- Caers J. Modeling uncertainty in the earth sciences. Boca Raton: Wiley; 2011.
- Calcagno P, Chilès JP, Courrioux G, Guillen A. Geological modelling from field data and geological knowledge. Part I. Modelling method coupling 3D potential-field interpolation and geological rules. *Phys Earth Planet Inter*. 2008;171(1–4):147–57. <https://doi.org/10.1016/j.pepi.2008.06.013>.
- Chen J, Hoversten GM, Key K, Nordquist G, Cumming W. Stochastic inversion of magnetotelluric data using a sharp boundary parameterization and application to a geothermal site. *Geophysics*. 2012;77(4):E265–79. <https://doi.org/10.1190/geo2011-0430.1>.
- Corbel S, Wellmann JF. Framework for multiple hypothesis testing improves the use of legacy data in structural geological modeling. *GeoResJ*. 2015;6:202–12. <https://doi.org/10.1016/j.grj.2015.04.001>.
- Crameri F. Geodynamic diagnostics, scientific visualisation and StagLab 3.0. *Geosci Model Dev*. 2018;11(6):2541–62.
- Cui T, Fox C, Sullivan MJO. Bayesian calibration of a large-scale geothermal reservoir model by a new adaptive delayed acceptance Metropolis Hastings algorithm. *Water Resour Res*. 2011;47:W10521. <https://doi.org/10.1029/2010W10521>.
- Cumming W. 3—Geophysics and resource conceptual models in geothermal exploration and development. In: Geothermal power generation. Amsterdam: Elsevier Ltd, p. 33–75; 2016 <https://doi.org/10.1016/B978-0-08-100337-4.00003-6>.
- De La Varga M, Wellmann F, Murdie R. Adding geological knowledge to improve uncertain geological models: a Bayesian perspective. *Geotecton Res*. 2015;97(1):18–20. <https://doi.org/10.1127/1864-5658/2015-08>.
- De La Varga M, Schaaf A, Wellmann F. GemPy 1.0: open-source stochastic geological modeling and Inversion. *Geosci Model Dev*. 2019;12:1–32.
- de Zeeuw-van Dalfsen E, Rymmer H, Williams-Jones G, Sturkell E, Sigmundsson F. Integration of micro-gravity and geodetic data to constrain shallow system mass changes at Krafla Volcano, N Iceland. *Bull Volcanol*. 2006;68(5):420–31. <https://doi.org/10.1007/s0445-005-0018-5>.
- Eggertsson G, Lavallée Y, Kendrick J, Markússon S. Improving fluid flow in geothermal reservoirs by thermal and mechanical stimulation: the case of krafla volcano, Iceland. *J Volcanol Geotherm Res*. 2018;. <https://doi.org/10.1016/j.jvolgeores.2018.04.008>.
- Einarsson P. S-wave shadows in the Krafla Caldera in NE-Iceland, evidence for a magma chamber in the crust. *Bull Volcanol*. 1978;41(1958):187–95.
- Einarsson P. Earthquakes and present-day tectonism in Iceland. *Tectonophysics*. 1991;189:261–79.
- Elders WA, Friðleifsson GO, Zierenberg RA, Pope EC, Mortensen AK, Guðmundsson A, Lowenstern JB, Marks NE, Owens L, Bird DK, Reed M, Olsen NJ, Schiffman P. Origin of a rhyolite that intruded a geothermal well while drilling at the Krafla volcano. Iceland. *Geology*. 2011;39(3):231–4. <https://doi.org/10.1130/G31393.1>.
- Elders WA, Friðleifsson GO, Albertsson A. Drilling into magma and the implications of the Iceland Deep Drilling Project (IDDP) for high-temperature geothermal systems worldwide. *Geothermics*. 2014;49:111–8. <https://doi.org/10.1016/j.geothermics.2013.05.001>.
- Fedi M, Rapolla A. 3-D inversion of gravity and magnetic data with depth resolution. *Geophysics*. 2002;64(2):452–60. <https://doi.org/10.1190/1.1444550>.
- Franzson H. Petrophysical properties of Icelandic rocks. In: Proceedings of the 6th Nordic symposium on petrophysics. 2001.
- Franzson H, Gudfinnsson G, Helgadottir H. Porosity, density and chemical composition relationships in altered Icelandic hyaloclastites. In: Torres-Alvarado I, Birkle P, editors. Water–Rock interaction, Frolova 2005. London: Taylor & Francis Group; 2010. p. 199–202.
- Frolova JV, Ladygin VM, Franzson H, Sigurðsson O, Stefánsson V, Shustrov V. Petrophysical properties of fresh to mildly altered hyaloclastite tuffs. In: World geothermal congress; 2005. April 24–29.
- Frolova YV. Specific features in the composition, structure, and properties of volcanoclastic rocks. *Moscow Univ Geol Bull*. 2008;63(1):28–37. <https://doi.org/10.3103/S0145875208010043>.
- Fullagar PK, Pears GA, McMonnies B. Constrained inversion of geologic surfaces—pushing the boundaries. *Lead Edge*. 2008;27(1):98–105. <https://doi.org/10.1190/1.2831686>.
- Garg SK, Pritchett JW, Wannamaker PE, Combs J. Characterization of geothermal reservoirs with electrical surveys : Beowawe geothermal field. *Geothermics*. 2007;36:487–517. <https://doi.org/10.1016/j.geothermics.2007.07.005>.
- Gasperikova E, Rosenkjaer GK, Arnason K, Newman GA, Lindsey NJ. Resistivity characterization of the Krafla and Hengill geothermal fields through 3D MT inverse modeling. *Geothermics*. 2015;57:246–57. <https://doi.org/10.1016/j.geothermics.2015.06.015>.

- Giraud J, Pakyuz-Charrier E, Jessell M, Lindsay M, Martin R, Ogarko V. Uncertainty reduction in joint inversion using geologically conditioned petrophysical constraints. *Geophysics*. 2017;82(6):1–61. <https://doi.org/10.1190/geo2016-0615.1>.
- Gudmundsson A. Formation and growth of normal faults at the divergent plate boundary in Iceland. *Terra Nova*. 1989;4:464–71.
- Gudmundsson MT, Högnadóttir T. Volcanic systems and calderas in the Vatnajökull region, central Iceland: Constraints on crustal structure from gravity data. *J Geodyn*. 2007;43(1):153–69. <https://doi.org/10.1016/j.jog.2006.09.015>.
- Gudmundsson MT, Milsom J. Gravity and magnetic studies of the subglacial Grímsvötn volcano, Iceland: Implications for crustal and thermal structure. *J Geophys Res*. 1997;102(B4):7691. <https://doi.org/10.1029/96JB03808>.
- Guillen A, Calcagno P, Courrioux G, Joly A, Ledru P. Geological modelling from field data and geological knowledge: part II. Modelling validation using gravity and magnetic data inversion. *Phys Earth Planet Inter*. 2008;171(1):158–69. <https://doi.org/10.1016/j.pepi.2008.06.014>.
- Hjartardóttir ÁR, Einarsson P, Bramham E, Wright TJ. The Krafla fissure swarm, Iceland, and its formation by rifting events. *Bull Volcanol*. 2012;74(9):2139–53. <https://doi.org/10.1007/s00445-012-0659-0>.
- Intrepid geophysics 3D GeoModeller reference. 2017a;
- Intrepid geophysics. Forward modelling and inversion with 3D GeoModeller. 2017b;
- Jessell M, Aillères L, Kemp ED, Lindsay M, Wellmann F, Hillier M, Laurent G, Carmichael T, Martin R. Next generation three-dimensional geologic modeling and inversion. *Soc Econ Geol*. 2014;18:261–72.
- Johnsen GV. Gravity map of the Krafla area (in Icelandic). In: Jónsson D, Jónsson SS, editors. *Hróarsson B. Gott mál hf: Eyjar í Eldhafi*; 1995. p. 93–100.
- Johnsen GV, Björnsson A, Sigurdsson S. Gravity and elevation changes caused by magma movement beneath the Krafla caldera, northeast Iceland. *J Geophys*. 1980;47(1–3):132–40.
- Jónasson K. Rhyolite volcanism in the krafla central volcano, north-east iceland. *Bull Volcanol*. 1994;56(6–7):516–28.
- Kaban MK, Flóvenz ÓG, Pálmason G. Nature of the crust-mantle transition zone and the thermal state of the upper mantle beneath Iceland from gravity modelling. *Geophys J Int*. 2002;149(2):281–99. <https://doi.org/10.1046/j.1365-246X.2002.01622.x>.
- Kennedy BM, Holohan EP, Stix J, Gravley DM, Davidson JR, Cole JW. Magma plumbing beneath collapse caldera volcanic systems. *Earth-Sci Rev*. 2018;177(December 2017):404–24. <https://doi.org/10.1016/j.earscirev.2017.12.002>.
- Khodayar M, Björnsson S, Kristinsson SG, Karlsdóttir R, Ólafsson M, Víkingsson S. Tectonic control of the Theistareykir geothermal field by Rift and transform zones in North Iceland: a multidisciplinary approach. *Open J Geol*. 2018;08(06):543–84. <https://doi.org/10.4236/ojg.2018.86033>.
- Kristmannsdóttir H. Alteration of basaltic rocks by hydrothermal activity at 100–300°C. *Dev Sedimentol*. 1979;27:359–67.
- Lévy L, Gibert B, Sigurdsson F, Flóvenz OG, Hersir GP, Briole P, Pezard PA. The role of smectites in the electrical conductivity of active hydrothermal systems: electrical properties of core samples from Krafla volcano, Iceland. *Geophys J Int*. 2018;215(3):1558–82. <https://doi.org/10.1093/gji/ggy342>.
- Li Y, Oldenburg DW. 3-D inversion of gravity data. *Geophysics*. 1998;63(1):109–19. <https://doi.org/10.1190/1.1444302>.
- Link WA, Eaton MJ. On thinning of chains in MCMC. *Methods Ecol Evol*. 2012;3(1):112–5. <https://doi.org/10.1111/j.2041-210X.2011.00131.x>.
- Maclaren OJ, Nicholson R, Bjarkason EK, O'Sullivan MJ. Incorporating posterior model discrepancy into a hierarchical framework to facilitate out-of-the-box mcmc sampling for geothermal inverse problems and uncertainty quantification. 2018; arXiv preprint [arXiv:181004350](https://arxiv.org/abs/181004350).
- Magnússon I (2016) Þyngdarmælingar á Peistareykjum í júl til september 2015 og Þyngdarkort af Kröflusvæði (Gravity measurements in Theistareykir in July–September 2015 and Gravity Map of the Krafla Area, in Icelandic). Tech. Rep. LV-2016-090, Iceland GeoSurvey, Reykjavik, Iceland, LV-2016-090.
- McCalman L, O'Callaghan ST, Reid A, Shen D, Carter S, Krieger L, Beardsmore GR, Bonilla EV, Ramos FT (2014) Distributed Bayesian geophysical inversions. In: Thirty-Ninth Stanford geothermal workshop. p. 1–11.
- Metropolis N, Rosenbluth AW, Rosenbluth MN, Teller AH, Teller E. Equation of state calculations by fast computing machines. *J Chem Phys*. 1953;21(6):1087–92.
- Miller CA, Williams-Jones G, Fournier D, Witter J. 3D gravity inversion and thermodynamic modelling reveal properties of shallow silicic magma reservoir beneath laguna del maule, chile. *Earth Planet Sci Lett*. 2017;459:14–27.
- Mortensen AK, Gudmundsson Á, Steingrímsson B, Sigurdsson F, Axelsson G, Ármannsson H, Björnsson H, Ágústsson K, Sæmundsson K, Ólafsson M, Karlsdóttir R, Halldórsdóttir S, Hauksson T, The Krafla geothermal system: a review of the geothermal system and a revised conceptual model (in Icelandic). Tech. rep. Landsvirkjun, Reykjavik, Iceland; 2009.
- Mortensen AK, Egilsson T, Gautason B, Árnadóttir S, Gudmundsson A. Stratigraphy, alteration mineralogy, permeability and temperature conditions of well IDDP-1, Krafla, NE-Iceland. *Geothermics*. 2014;49:31–41. <https://doi.org/10.1016/j.geothermics.2013.09.013>.
- Mosegaard K, Tarantola A. Monte Carlo sampling of solutions to inverse problems. *J Geophys Res Solid Earth*. 1995;100(B7):12431–47. <https://doi.org/10.1029/94JB03097>.
- Nono F, Gibert B, Parat F, Loggia D, Cichy SB, Violay M. Electrical conductivity of Icelandic deep geothermal reservoirs up to supercritical conditions: insight from laboratory experiments. *J Volcanol Geotherm Res*. 2018; <https://doi.org/10.1016/j.jvolgeores.2018.04.021>.
- Ochs FA, Lange RA. The density of hydrous magmatic liquids. *Science*. 1999;283(5406):1314–7. <https://doi.org/10.1126/science.283.5406.1314>.
- Olierook HKH, Scalzo R, Kohn D, Chandra R, Farahbakhsh E, Houseman G, Clark C, Reddy SM, Müller RD. Bayesian geological and geophysical data fusion for the construction and uncertainty quantification of 3D geological models. *Solid Earth Discuss*. 2019;January:1–34. <https://doi.org/10.5194/se-2019-4>.
- Oliver Ocaño FM, Gallardo LA, Romo-Jones JM, Perez-Flores MA. Structure of the Cerro Prieto Pull-apart basin from joint inversion of gravity, magnetic and magnetotelluric data. *J Appl Geophys*. 2019; <https://doi.org/10.1016/j.jappgeo.2019.103835>.
- Opheim J, Gudmundsson A. Formation and geometry of fractures, and related volcanism of the Krafla fissure swarm, northeast Iceland. *Soc Am Bull*. 1989;101(12):1608–22.

- Pearson-Grant SC, Franz P, Clearwater J. Gravity measurements as a calibration tool for geothermal reservoir modelling. *Geothermics*. 2018;73(December 2016):146–57. <https://doi.org/10.1016/j.geothermics.2017.06.006>.
- Pope EC, Bird D, Arnorsson S, Giroud N. Hydrogeology of the Krafla geothermal system, northeast Iceland. *Geofluids*. 2016;16(1):175–97.
- Rosas-Carbajal M, Linde N, Peacock J, Zyserman FI, Kalscheuer T, Thiel S. Probabilistic 3-D time-lapse inversion of magnetotelluric data: application to an enhanced geothermal system. *Geophys J Int*. 2015;203(3):1946–60. <https://doi.org/10.1093/gji/ggv406>.
- Rosenkjaer GK, Gasperikova E, Newman GA, Arnason K, Lindsey NJ. Comparison of 3D MT inversions for geothermal exploration: case studies for Krafla and Hengill geothermal systems in Iceland. *Geothermics*. 2015;57:258–74. <https://doi.org/10.1016/j.geothermics.2015.06.001>.
- Rymer H, Tryggvason E. Gravity and elevation changes at Askja, Iceland. *Bull Volcanol*. 1993;55:362–71.
- Rymer H, Cassidy J, Locke CA, Sigmundsson F. Post-eruptive gravity changes from 1990 to 1996 at Krafla volcano, Iceland. *J Volcanol Geotherm Res*. 1998;87(1–4):141–9. [https://doi.org/10.1016/S0377-0273\(98\)00092-4](https://doi.org/10.1016/S0377-0273(98)00092-4).
- Sæmundsson K. Geology of the Krafla system. *The Natural History of Lake Myvatn*, 1991; p. 24–95.
- Sæmundsson K. Krafla. *Geological Map*, 1:25000. Tech. rep., Landsvirkjun and Iceland GeoSurvey, Reykjavik, Iceland. 2008.
- Scales JA, Tenorio L. Prior information and uncertainty in inverse problems. *Geophysics*. 2001;66(2):389–97. <https://doi.org/10.1190/1.1444930>.
- Scott S, Driesner T, Weis P. Geologic controls on supercritical geothermal resources above magmatic intrusions. *Nat Commun*. 2015; <https://doi.org/10.1038/ncomms8837>.
- Scott S, Driesner T, Weis P. The thermal structure and temporal evolution of high-enthalpy geothermal systems. *Geothermics*. 2016;62:33–47. <https://doi.org/10.1016/j.geothermics.2016.02.004>.
- Shannon CE. A mathematical theory of communication. *Bell Syst Tech J*. 1948;27(3):379–423.
- Sigurðsson Ó, Guðmundsson Á, Friðleifsson GÓ, Franzson H, Guðlaugsson S, Stefánsson V. Database on igneous rock properties in Icelandic geothermal systems. Status and unexpected results. In: *Proceedings world geothermal congress*. 2000; p. 2881–2886.
- Soyer W, Mackie R, Hallinan S, Pavesi A, Nordquist G, Suminar A, Intani R, Nelson C. Multi-Physics Imaging of the Darajat Field. *GRC Transactions*. 2017; 41.
- Stefánsson V. The Krafla geothermal field, northeast Iceland. In: Rybach L, Muffler LJP, editors. *Geothermal systems: principles and case studies*. New York: Wiley-Interscience; 1981. p. 273–93.
- Sveinbjörnsdóttir Á. Composition of geothermal minerals from saline and dilute fluids-Krafla and Reykjanes, Iceland. *Lithos*. 1992;27:301–15.
- Tarantola A. Popper, Bayes and the inverse problem. *Nat Phys*. 2006;2(8):492–4. <https://doi.org/10.1038/nphys375>.
- Thien BMJ, Kosakowski G, Da Kulik. Differential alteration of basaltic lava flows and hyaloclastites in Icelandic hydrothermal systems. *Geotherm Energy*. 2015;3(1):11. <https://doi.org/10.1186/s40517-015-0031-7>.
- Tryggvason E. Multiple magma reservoirs in a rift zone volcano: ground deformation and magma transport during the September 1984 eruption of Krafla, Iceland. *J Volcanol Geotherm Res*. 1986;28(1):1–44.
- United Nations Economic Commission for Europe Expert Group on Resource Classification. *Application of UNFC to Geothermal Energy Resources—Selected case studies*. United Nations: Tech. rep; 2017.
- Walker GPL. Compound and simple lava flows and flood basalts. *Bull Volcanol*. 1971;35:579–90. <https://doi.org/10.1007/BF02596829>.
- Weisenberger TB, Axelsson G, Arnaldsson A, Blischke A, Óskarsson F, Ármannsson H, Blanck H, Helgadóttir HM, Berthet JCC, Arnason K, Ágústsson K, Gylfadóttir SS, Guðmundsdóttir V. Revision of the Conceptual Model of the Krafla Geothermal System. Tech. rep., Landsvirkjun, Reykjavik, Iceland. 2015.
- Wellmann JF, Regenauer-Lieb K. Uncertainties have a meaning: information entropy as a quality measure for 3-D geological models. *Tectonophysics*. 2012;526–529:207–16. <https://doi.org/10.1016/j.tecto.2011.05.001>.
- Wellmann JF, De La Varga M, Murdie RE, Gessner K, Jessell M. Uncertainty estimation for a geological model of the Sandstone greenstone belt, Western Australia—insights from integrated geological and geophysical inversion in a Bayesian inference framework. *Geological Society*. 2017;453:SP453–12.
- Williams DL, Finn C. 28. Analysis of gravity data in volcanic terrain and gravity anomalies and subvolcanic intrusions in the cascade range, USA, and at other selected volcanoes. In: *The utility of regional gravity and magnetic anomaly maps, general series, society of exploration geophysicists*. 1985; p. 361–74. <https://doi.org/10.1190/1.0931830346.ch28>.
- Witter JB, Siler DL, Faulds JE, Hinz NH (2016) 3D geophysical inversion modeling of gravity data to test the 3D geologic model of the Bradys geothermal area, Nevada, USA. *Geotherm Energy*. <https://doi.org/10.1186/s40517-016-0056-6>.

## Publisher's Note

Springer Nature remains neutral with regard to jurisdictional claims in published maps and institutional affiliations.